4.2 Linac Technology

4.2.1 The Accelerating Section

The main goal of the accelerating structure is, to transform rf-power to beam power in an efficient manner. On the other hand, given the frequency, only small improvements over a typical S-Band section are possible in terms of shunt impedance, Q-value or resonator geometry. Therefore the design is mainly guided by the necessity to control the longitudinal and transverse wakefields. The production on the other hand has to guarantee ultra-clean structures in order to achieve high gradients with small dark currents and excellent vacuum conditions. Several aspects, which are essential for both items, are still under investigation and aim for minimum linear costs of the production of approximately 5000 sections in a 30 kilometer long collider.

The design of the accelerating section has been developed during the R & D program for the S-Band Linear Collider Test Facility at DESY which started in 1992. Four accelerating structures for the test facility are under production which fulfill the requirements of a linear collider. In addition many technological aspects have been worked out during the production of spare accelerating structures for the injector linac at DESY (LINAC II) where overall fourteen sections have to be replaced because of corrosion in the cooling system. The main parameters of both structures are listed in Table 4.2.1. From the production and operation of these two types of accelerationg sections sufficient experience has been aquired to extrapolate to a large scale series production. During operation of these sections, especially those for the test facility, the aspects which are essential for the linear collider are investigated and will be discussed in more detail in the following part.

section parameter			
		L C	Linac II
section length	m	6	5.2
attenuation	neper	0.55	0.5
group velocity variation	% of c	4.1–1.3	3.3–1.2
filling time	nsec	790	750
shunt imped. variation	MΩ/m	45–61	52–62
number of cells		180	156
tolerances			
straigthness over 6 m	μm rms	≈ 50	$\approx \leq 500$
alignment	μm rms	≤ 50	≤ 1000

Table 4.2.1: *Parameters of the S-Band Linear Collider Section and the Linac II sections, both built at DESY.*

The straightness and alignment tolerances which are quoted later on in this part mainly result from tracking calculations. These calculations are described in great detail in section 4.3. They are based on the longitudinal and transverse wakefields which have mainly been calculated and partly measured in accelerating structures. While the order of magnitude of the wakefields is essentially determined by the choice of the operating frequency, the effective long range wakefield can be reduced with HOM dampers, internal damping and/or detuning. These strategies are an integral part of the design of the S-Band Linear Collider section and the different aspects concerning the design and fabrication will be presented in detail.

Other isssues are the design and construction of a small size symmetric high power coupler which has been proposed and built for the test facility structures. The collinear load, a design copied from the old LINAC II sections replaces the coupler at the output end and guarantees a good rf match as well as perfect symmetry to avoid transverse kicks in the coupler cell, has been redeveloped and new production techniques have been applied. Finally the design of the Higher Order Mode (HOM) couplers is still ongoing and size and complexity has to be further reduced to make application of modern production and assembly techniques possible.

4.2.1.1 Structure Design

The choice of the accelerating gradient is determined by a balance of linear costs as compared to costs which apply to the rf system. For the S-Band Linear Collider study, with the assumptions which have been made and the cost basis which is available already, this leads to broad optimum around a gradient of 20 MV/m. Given the shunt impedance, mainly determined by the choice of the operating frequency of 3 GHz and the peak power available from one power source, based on today's available technology, one klystron can feed roughly 12 m of accelerating structure.

The reason to choose 6 m long accelerating sections as compared to the well known 3 m long structure from SLAC, is the reduced number of couplers, input windows or valves and a simpler power distribution system. On the other hand, with longer sections and a fixed filling time, the average iris diameter increases which reduces the attainable shunt impedance. This results in a trade-off between loss in average shunt impedance using long rf-sections as well as constructional feasibility versus a larger number of input couplers and a more complex rf power distribution system. Having in mind a future energy upgrade by doubling the number of klystrons, which is the maximum to be expected, underlines this decision because every section may then be connected to one klystron.

Each section is equipped with one high power coupler. The high power coupler is symmetric and has a power splitter on top. The symmetry of the coupler minimizes the amplitude and phase assymmetry. In additon the power transmission per coupling iris is reduced. The output power is not extracted through an output coupler but sufficiently absorbed in an integrated load, which consists of the last eight accelerating cells of the travelling wave structure.

The behaviour of the wakefield in this type of accelerating structure has been investigated in much more detail during the last years R & D for Linear Colliders. The total long range wakefield is given by the sum of all modes in each passband of the structure. Because the geometry is changed from cell to cell in, for example, a standard constant gradient structure, the electric field pattern and correspondingly the interaction with the beam is quite complex. The frequency spread which is introduced due to these geometric variations, naturally detunes the long range wakefield on a time scale given by the width of the frequency distribution.

This effect of decoherence of the long range wakefield is a part of the design philosophy of the S-Band accelerating structure and is described in greater detail in part 4.2.1.4. Detuning is achieved by variation of the cell to cell frequency of higher order modes to decohere the wakefield on a time scale given by the bunch to bunch spacing of 6 nsec. For example, the first dipole mode single cell frequency changes by approximately 300 MHz from the front to the back end of the structure. In addition ten classes of structures have to be produced which are slightly varied in geometry compared to each other. Here identical modes are shifted in frequency with a total scatter from structure to structure of 36 MHz. This further reduces the beam instability.

Finally each structure is equipped with two HOM pick-ups, which are waveguide type couplers (used in the test facility) or simple coupling loops, which are frequency selective. The pick-up is used to determine to power induced into dipole modes. This information will further on be used to align the structure with respect to the beam axis. Each of the two pick-ups will feedback to a micro mover placed at both ends of the girder. The section is mechanically decoupled from the next quadrupole or the next chamber with bellows which allow transverse displacemnts over the full range of the mover (± 1.5 mm).

4.2.1.2 Structure Fabrication

Given the tolerances and the rf design of the linear collider section, reduction of the fabrication costs for the accelerating sections of a Linear Collider (LC) is one of the figures of merit of the production. Accelerating strucutres for the test facility and for the injector linac at DESY (LINAC II) have been produced using different production techniques. Both sections are quite similar apart from the fact that the straightness tolerances are larger by approximately an order of magnitude for LINAC II. For comparison the parameters are given in table 4.2.1.

Cell Design The six meter long disc loaded LC structure consists of 179 single cups and the coupler cell. Due to the comparatively simple geometry of the disc loaded structure the strategy was to use single cell shapes to be produced easily by conventional machining with reasonable tolerances. The shape of the cavity itself and of the outside walls are a compromise between simplicity and mechanical or rf-requirements.

- The cells should be machined in one piece to form *cups* instead of having a ring and an iris seperately. The cups nest into each other to perform a self alignment during assembly. Especially during vertical brazes, the self-aligning should provide reasonably straight pieces of structures of 0.8-1.5 meter length.

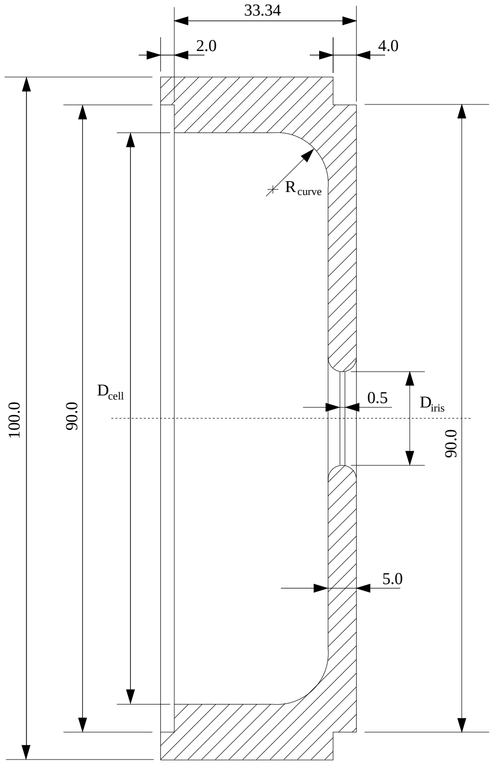

Figure 4.2.1: *Single Cell Geometry.*

- The electric contact between two cups is defined by the copper on copper junction to provide excellent rf properties (high Q values). A knife edge type copper to copper contact prevents any brazing material to penetrate into the cell.

- The tolerance on the outer wall diameter of the cavity has to be similar to the inner cavity wall- and the iris diameter to measure and confirm the straightness with respect to the electrical axis.

Specified tolerances are $\pm 10\,\mu$m for the most sensitive dimensions, namely the cavity diameter and the iris diameter, while tolerances measured so far on average with a statistics of about 2000 cups indicates that less than $\pm 2\,\mu$m can be achieved easily. The specified tolerances have been chosen by the maximum tuning range on one cell while the achieved tolerances are already attractive enough in order not to tune but only to measure the elctrodynamic characteristics of each of the 5000 required sections. The resulting energy loss is less than 1 %, if the section can be operated without any sytematic phase error and is left with the statistical error only. This will be achieved by operating each structure at its optimum temperature, which is expected to vary by less than ± 1 C° from section to section. The cooling system is designed to handle this feature (see 4.2.4. A significant financial and operational gain is expected because the cup does not need any tuning holes in the outside wall and the production time will be reduced because the time consuming tuning procedure is not required.

Material Handling, Preparation and Assembly The cups itself are machined from forged copper pieces and chemically cleaned afterwards. To improve the outgassing rate and to decrease potential contaminations of the raw copper material, Hot Isostatic Pressure (HIP) procedures have been applied and intensively investigated elsewhere [1]. At a gradient larger than 75 MV/m a dark current of less than 1 mA has been measured. Additional experiments at KEK have proven that dark currents produced by field emission can be reduced by more than an order of magnitude if clean room conditions and high pressure water rinsing is applied. At DESY significant effort has been put into the research of material aspects and the material preperation during production in order to reduce the amount of gas stored in the metal and to increase the breakdown threshold. According to both results different types of pretreated structures have to be tested and the cause of dark current production must be traced using the test facility and the available high power test stands.

Substructrures are preassembled and brazed vertically in pieces of approximately 0.8 m length, which are vacuum checked each. The straightness achieved on these pieces is generally better than 30 μm without additional supports. Longer pieces up to the full structure length will be brazed vertically as well to avoid support strcutures. The stra

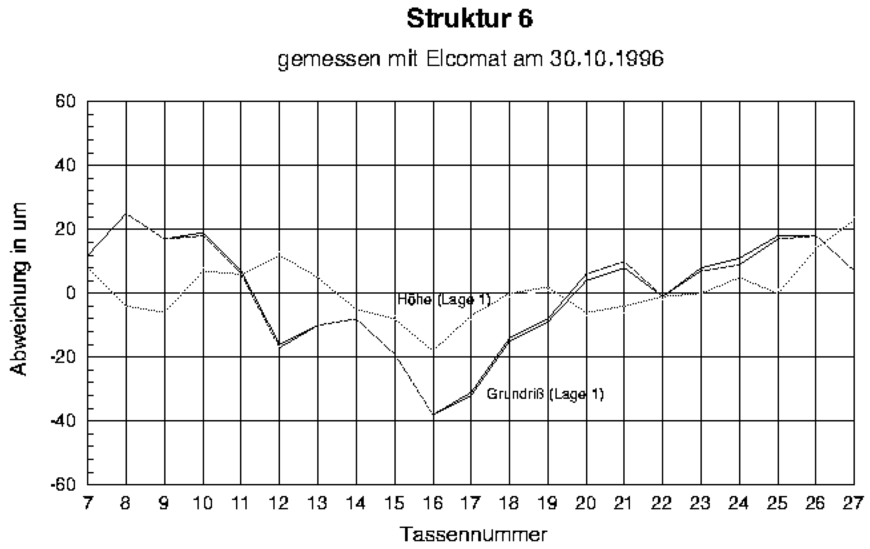

Figure 4.2.2: *Straightness of a 1 meter long piece of accelerating structure brazed vertically without further supports. (Höhe: vertical)*

A new method, namely inductive heating, which is has been investigated recently fullfils almost all requirements for the large series production of more than 5000 sections. Heat-up and cool-down procedures can be applied while the structure is mounted vertically within a small glass or ceramic pipe flooded by hydrogen. Already with the available hardware at DESY the time required for brazing is approximately half an hour per meter.

Straightening of Accelerating Structures Apart from the electrodynamic characteritics of the accelerating structure, the straightness is a main concern in the linear collider design. The straightness tolerance is mainly given by the multibunch instability threshold which is driven by dipole modes. These modes will be excited even if the average offset of the single cells is zero. In case of tapered structures, constant gradient, gaussian or others, these dipole modes of one passband are loacated at different places in the section. The minimum length for which the straightness is defined is determined by that part of the electric field of each dipole mode which is strongly interacting with the beam, typically 40 cm–60 cm. The desirable straightness tolerance defined from this criterion is: **The section has to be straight over the 6 m length to within 30 μm rms over a length larger than 60 cm.** For longer pieces slightly larger values can be accepted which will later on be removed. This is smaller by a factor of two than actually required for the 500 GeV collider design, but takes into account that future upgrades require the acceleration of smaller emittance beams. A measurement showing a 1 meter long piece brazed vertically is shown in Fig. 4.2.2.

Heating the copper during the braze up to ≈900 C° reduces the young's modulus by almost factor of three. Detoriation of the straightness would require more than one support per meter in order to fix the section with the required straightness on the final girder. Straightening the section, if necessary, after the final braze is a more attractive and envisaged solution. A straightening device used for the test structures together with a fast laser measurement system has been constructed and is under test. A sketch is shown in Fig. 4.2.3.

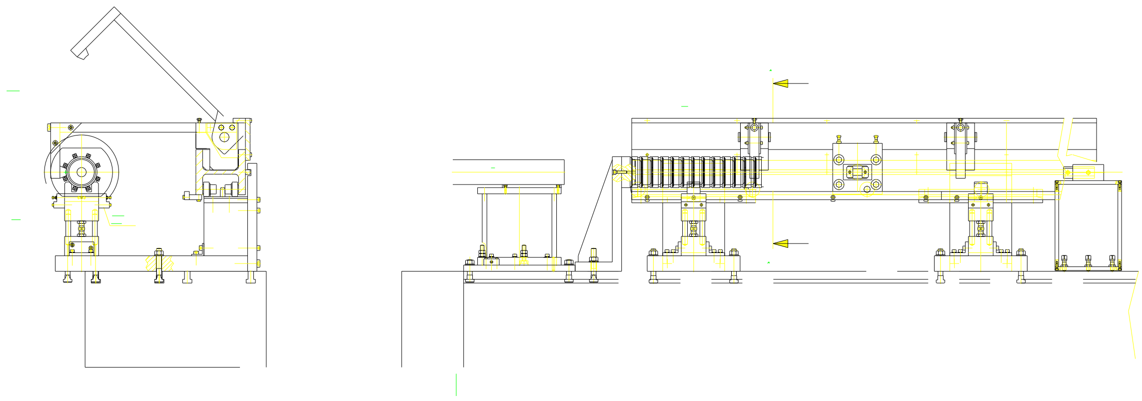

Figure 4.2.3: *Device for straightening of the accelerating sections after the final braze and before installation on the girder.*

Straightness Measurement Techniques In the following text alignment techniques are discussed which are used to control the straightness of a structure. Certainly other techniques can be used and they are described for example in [2].

Straightness Measurement using an Interferometer For straightness measurements in combination with the straightening device a normal laser interferometer is used. In addition to the laser head and the measurement display unit for straightness measurements, a straightness interferometer (compensated wollaston prism) and a mirror (straightness reflector) are also required. The function principle is described in [3]. The mirror is mounted on a fixed support behind the module and the wollaston prism runs along the module. The offset distance of the wollaston prism in horizontal or vertical direction with respect to a straight reference line will be measured, in that the reference line will be given by the mirror axis and not by the laser beam.

At DESY the laser interferometer system HP 5528 A is available. There are two straightness interferometers, one for the short range up to 3 m and another for the long range from 1 m to 30 m. In both systems the measurement range is ± 1.5 mm and the resolution is better than 0.1 μm. The accuracy of the short range interferometer is between 3.5% and 1% and of the long range interferometer between 5% and 2.5% of the measured offset. With an interferometer, only one geometrical position can be measured either the vertical or the horizontal position. During the measurement care must be taken not to move the wollaston prism out of the laser beam or to interrupt the laser beam itself.

Straightness Measurement using Autocollimator An autocollimator can measure the changes in direction of a surface mirror with very high accuracy. For straightness measurement using autocollimation a surface mirror is mounted in a sliding carriage running in defined steps along the module. In each position of the sliding carriage the vertical and the horizontal directions of the mirror axis will be measured by the autocollimator (Fig. 4.2.4). This method is used for the final measurement of the straightness on the actual girder.

The changes in direction for each component in respect of the first mirror position multiplied by the distance of the supporting points of the sliding carriage are accumulated. Therefore the straightness curve of the module can be calculated. By the autocollimator technique in one process horizontal and vertical straightness deviations will be measured simultaneously. This is an important advantage compared to the two straightness measuring techniques described previously. Furthermore there is no laser beam to interrupt and it is possible to put the sliding carriage out of the field of vision of the autocollimator completely. The effects of refraction of air have also to be taken into account. Further it can be seen that the supporting points of the sliding carriage are pressed into the module by the weight irregularly. The weight of the carriage and the surface mirror must therefore be as low as possible.

At DESY the autocollimator Elcomat 2000 of the factory Möller–Wedel in Wedel is used. This electronic autocollimator has in the focal plane two CCD–line scan image sensors mounted perpendicular to each other to detect the crosshair reflecting from

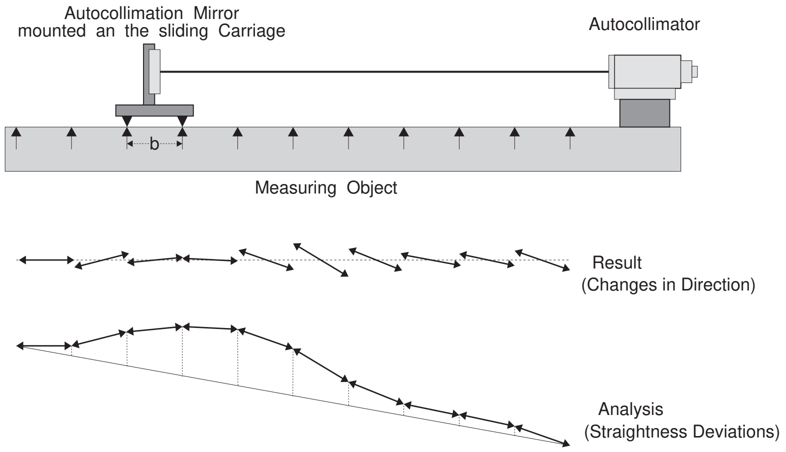

Figure 4.2.4: *Sketch of a straightness measurement using an autocollimator. Changes in direction from point to point, which are given by the angle of the reflected laser beam with respect to the surface of the mirror, are used to determine the transvese offset in both planes.*

the surface mirror automatically. The measuring range is $\pm 1000''$. With increasing distance between autocollimator und surface mirror the measuring range will decrease. For a distance of 3 m the measuring range is now $\pm 500''$ and for a distance of 7.5 m the measuring range is only $\pm 100''$. The accuracy of the Elcomat is between $0.15''$ and $0.50''$.

In [3] the results of several straightness measurements carried out with the described systems are discussed. Fig. 4.2.5 shows the remaining deviations of a 5.2 meter structure after the first straightening the module, where an rms value of 107 and 108 μm in the vertical and horizontal plane has been achieved.

4.2.1.3 Input Coupler and Collinear Load

Description of the Problem The rf power P_{in}, which is provided by a standard rectangular WR284 S-band waveguide, is converted to the traveling accelerating mode in the first cell of the disc loaded structure. The main design issues for the coupler are the symmetry of the accelerating field, the proper amplitude and phase relationship to the rest of the structure, the high power capability (300 MW for the 1 TeV version), perfect matching at the input port and a compact design to save tunnel space. The end of the accelerating section has to be terminated for the accelerating traveling wave to avoid increased electrical peak field strengths, reflections back to the klystron, and to reach the desired traveling wave operation. Therefore the power left over at the end of the structure has either to be extracted by an output coupler to an external load, or to be dissipated in the last few cells which act as an internal load. The internal load - called collinear load - has to fulfill the termination condition and to work simulataneously as accelerating structure.

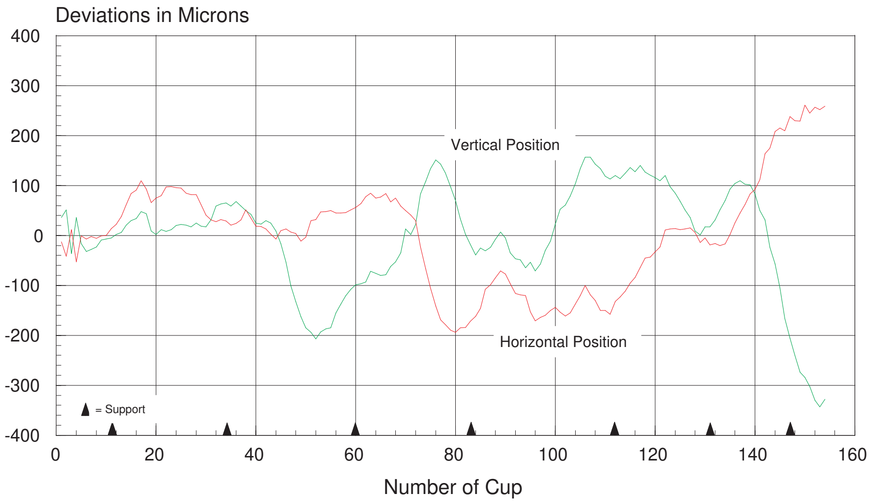

Figure 4.2.5: *Straightness deviations of a 5.2 meter long structure after straightening the module. Seven arrows on the bottom of the graph indicate the suppport points.*

Technical Solutions for the Coupler Arrangements with only one coupling hole at the circumference of the first cell introduce intolerable phase and amplitude asymmetries in the coupler fields with which the beam interacts. The field distortion can be reduced by asymmetric arrangements of the coupler cell with respect to the beam axis or by using compensation elements on the side opposite to the coupling hole [4, 5]. However, the compensation is still imperfect and the transient field in a single coupling hole can be quite large. This can be avoided by input couplers with two coupling holes which are symmetric in the vertical and horizontal plane with respect to the beam axis. In [6] a setup is described where two coupling irises are fed in phase by signals from a power divider. Each iris transmits one half of the total power flow. Very compact designs are possible with side coupled waveguides as it can be seen in Fig. 4.2.6. The symmetry of this configurations is not quite perfect with respect to the horizontal plane, but the field error in the coupler cell is sufficiently reduced.

Side Coupled Input Coupler A high power coupler with two side coupled waveguides has been developed in collaboration with MEPhI in Moscow [7]. The design in Fig. 4.2.6 is composed by two independent units which are connected by vacuum flanges:

- few centimeters for the cut-off pipe, the first two cells of the accelerating structure, the side coupled waveguides terminated on one side by a conducting plane and
- the power splitter, a $\lambda/2$ taper from the cell height of 28.34mm to the height of the standard S band waveguide (34.04mm) and a diaphragm.

The following properties have been measured at the prototype:

- input reflection coefficient below 1.5% ,

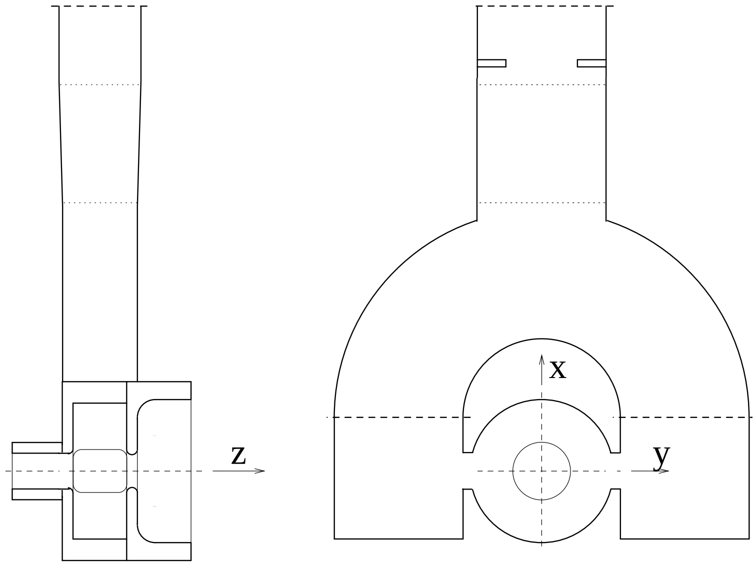

Figure 4.2.6: *Geometry of side coupled symmetric input coupler with power splitter and tapered waveguide.*

- the peak field strength in the coupling hole is 65% of the accelerating field,
- the amplitude- and phase asymmetry are of the order of the measurement accuracy ($(\partial|E_z|/\partial x)/|E_z| = 0.009$/mm, $\partial arg(E_z)/\partial x = 0.035$ degree/mm)

Hybrid Input- and HOM-Coupler The possibilities of using additional coupling elements at the first cell in order to damp or detect higher order modes have been investigated in theory and with an experimental setup [8]. A sketch of the modified coupler can be seen in Fig. 4.2.7: the conducting terminations at side coupled waveguides have been replaced by two waveguides below cutoff frequency which provide the same reflection coefficient. These waveguides are operated above the cutoff frequency for dipole modes, so that their energy can be absorbed at the terminating loads. Dipole modes with orthogonal polarization couple through two additional holes to a second pair of waveguides. With such a configuration it is possible to decrease the quality factor of dipole modes with both polarizations by a factor 5 while maintaining the match at the fundamental mode frequency. This coupler has been investigated as an alternative approach compared to the HOM dampers which are connected to the cells. This solution has not been chosen due to its complexity and because a large number of modes of the 1st dipole band are trapped apart from the coupler (compare Sect. 4.2.1.4).

The Collinear Load The collinear load, which is proposed instead of an output coupler, consists of the last eight accelerator cells. The surface losses in these cells are artificially increased by an ≈0.1 mm thick layer of Kanthal. The quality factor of these cells can be decreased in a controlled fashion by a factor of almost 50. The parameters

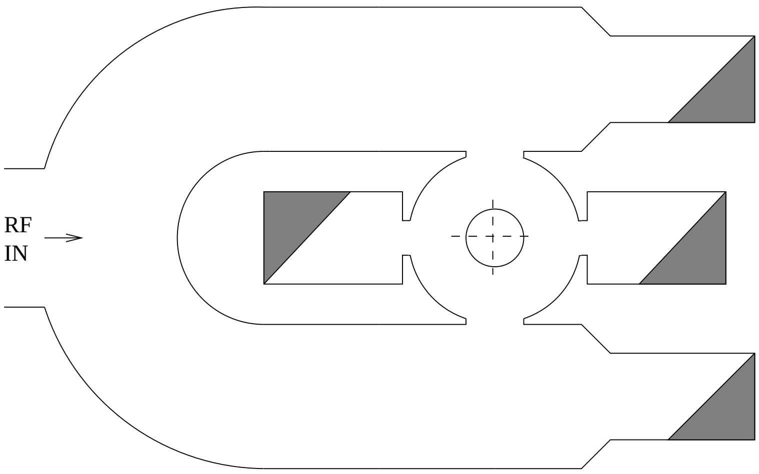

Figure 4.2.7: *Hybrid coupler.*

of each cell (frequency, coupling and quality) are optimised to fulfill the termination condition and to be close to the desired amplitude and phase distribution. An other criterium for the optimization is the power dissipation along the load. Apart from the fact that significant cost savings have been achieved, using a collinear load has a number of advantages as compared to a standard output coupler:

- The collinear load is perfectly symmetric which avoids transverse excitation of the beam and intrinsically does not contribute to any emittance growth.
- All the higher order modes with field in the last few cells are automatically damped via losses in the cavity walls.
- No output coupler together with a load is required which reduces the failure risk significantly.
- The loss in linear length is neglegible because the particles are still accelerated in the collinear load.

4.2.1.4 Higher Order Mode Damping and Detection

Deterioration of the intense particle beams in a multibunch collider scheme is caused by the long range wake fields. Theses deflecting fields build up by parasitic higher order modes (HOMs) in the accelerating structures which have been excited by preceeding bunches. If no special damping is applied the energy of the beam induced fields will be dissipated by wall losses (in the cells or the collinear load), propagate through the beam pipe or through the high power coupler. Because the energy propagation through the beam pipe leads only to an exchange of rf power between adjacent structures this mechanism does not really cause damping unless beam pipe absorbers are present. Due to the existance of modes which are completely trapped inside a section (compare Figure 4.2.8) and due to the low velocity of energy propagation (typically few percent of the velocity of light) many modes are only damped by wall losses. In this case an upper limit for the decay time τ can be estimated using the asymptotic limit of a pill box resonator:

$$\tau = \frac{r_{cell}}{\pi f_\nu \sigma}$$

with r_{cell}=cell radius, f_ν=mode frequency and σ= skin depth. Therefore even for frequencies much higher than the fundamental mode, decay times in the order of microseconds have to be expected.

The dominant and lowest order contributions to the longitudinal and transverse wake are related to monopole and dipole fields. The longitudinal monopole effects are independent from offsets between the beam and section axis induced for example due to the injection offsets and alignment errors of structures and quadrupoles. Therefore they are predictable and can be compensated easily (see Sect. 4.2.9) or are negligible. In contrast to this, dipole mode effects depend strongly on geometric errors and require special structure designs to prevent multibunch beam break-up and emittance dilution. A key quantity for the analysis of these effects is the normalized transverse dipole wake $w_D(s)$ which is related to the change of the transverse momentum $\Delta\mathbf{P}_t$ of a test charge q_2 caused by the fields of a source bunch q_1 by:

$$\Delta\mathbf{P}_t = w_D(s) \cdot \frac{q_1 q_2}{c} \mathbf{r}_{1t} \ ,$$

$\mathbf{r}_{1t}$ is the transverse offset of the drive charge with respect to the structure axis and s is the distance between q_1 and q_2.

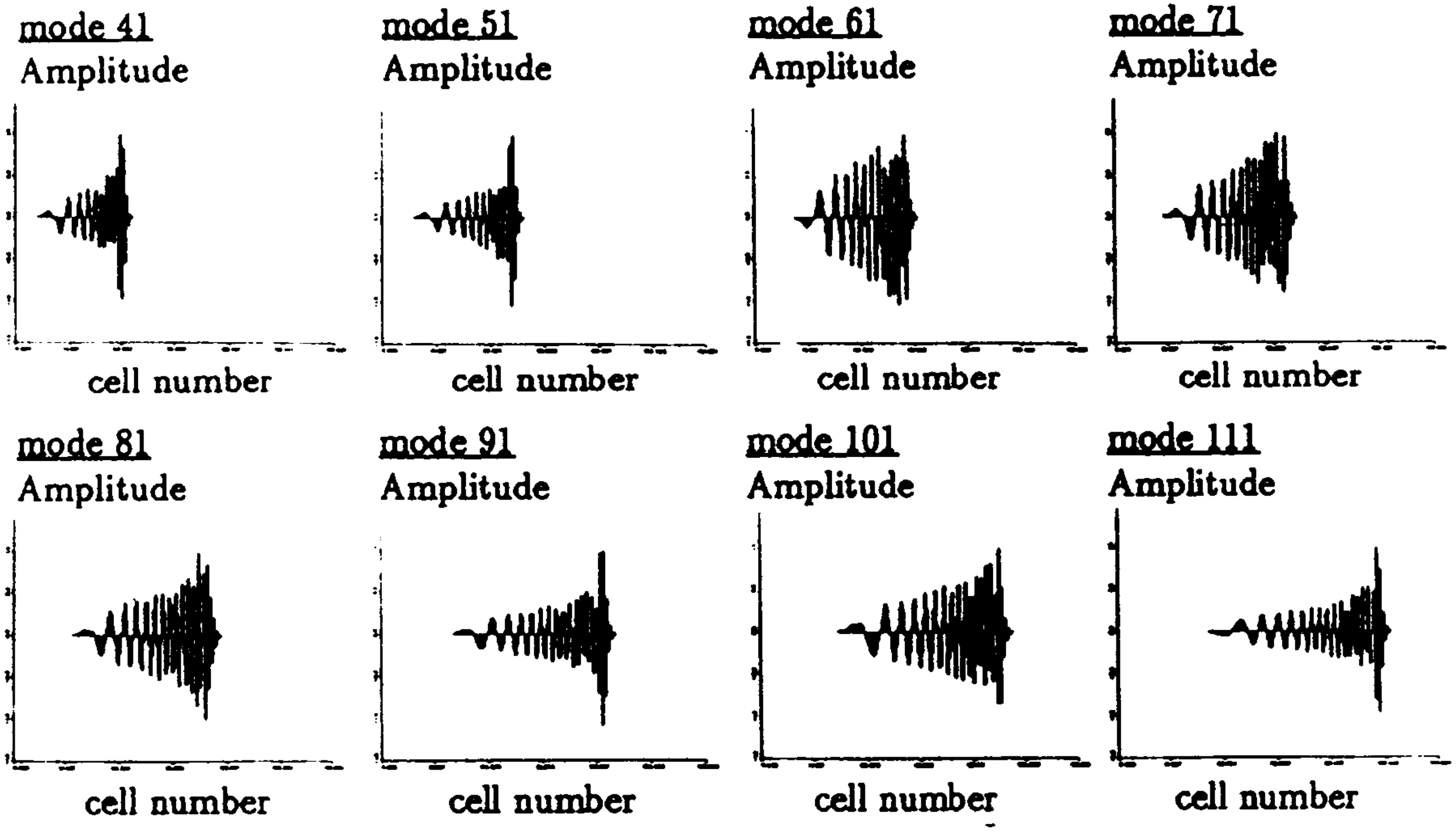

Figure 4.2.8: Normalized voltage amplitudes of some trapped HOMs in the 180-cell quasi-constant gradient structure as function of cell number.

Computation of the Dipole Long Range Wake The normalized transverse dipole wake function $w_D(s)$ can be split into a resonant term $w_r(s)$ and a transient term $w_t(s)$. The resonant part can be expressed by a summation over all eigenmodes ν:

$$w_r(s) = \sum_{\nu} 2k'_{\nu} \frac{c}{2\pi f_{\nu}} \sin\left(\frac{2\pi f_{\nu}}{c} s\right) \quad \text{for} \;\; s > 0,$$

where f_{ν} and k'_{ν} denote the resonance frequency and the normalized longitidinal loss-parameter (definition see [10]) corresponding to the ν-th cavity mode. Usually this equation is modified by damping terms with the time constants $\tau_{\nu} = Q_{\nu}/(\pi f_{\nu})$ to take into account small losses e.g. due to the finite wall conductivity.

The application of grid-oriented methods for tapered disc-loaded structures is limited by the realizable number of mesh points and the accuracy of the eigenvalue solver. Semi-analytical methods like the Modal Field Matching Technique do not suffer from this limitation and can be applied for the HOM calculation [10]. To make the problem tractable the 180 cell constant gradient structure of the SBLC Design was approximated by a 180 cell model which is tapered in groups of six cells with rectangular instead of rounded corners [10]. In order to further study the phenomenon of trapped modes a 36-cell structure has been designed [11] and a double-band coupled oscillator model has been developed. The parameters f_{ν}, k'_{ν} and Q_{ν} of the resonant wake and the complete function $w_D(s)$ have been calculated and compared by different methods:

- Calculation of f_{ν} and k'_{ν} in the frequency range 4.1 GHz to 4.6 GHz for a piecewise tapered section (in groups of six) using the mode matching technique [10]. The electric field distributions of the modes which have been found in this frequency range correspond to those which are given from the first and part of the second dipole passband, taking the individual cells in periodic approximation. The individual passbands with the dispersion curves for the first, the last cell and some cells in between are shown in fig 4.2.9. The plot displayed in Figure 4.2.10 shows a scatter (due to the piecewise tapered geometry being used) of the loss factors between 2 and 14×10^{15} extended over 2/3 of the first dipole passband. A major part of these modes is trapped *inside* the structure, that is without contact to the end cells which can be seen from the electric field distributions of the modes as well (compare Figure 4.2.8). This loss-parameter distribution has been used for the beem dynamics simulations in [9, 16].

- Calculation of f_{ν} and k'_{ν} in the frequency ranges from 4.1 GHz to 4.6 GHz and from 9.3 GHz to 9.4 GHz using the mode matching technique [18]. The modes in the second frequency range correspond to the sixth dipole passband, which significantly contributes to the impedance of the structure.

- Calculation of f_{ν}, k'_{ν} and Q_{ν} in the frequency range of the first and second passband (4.1 GHz to 5.6 GHz) by a double-band coupled oscillator model [20]. This model takes into account weak and strong losses (e.g. wall losses, HOM couplers). The loss-parameter distribution of the disc loaded SBLC-section without couplers and collinear load is plotted in Fig. 4.2.11 and can be directly compared to fig. 4.2.10.

- Calculation of $w_D(s)$ in the frequency range below 15 GHz in time domain [9].

In addition the computation methods [10, 18, 20] have been verified by a comparison with finite-integration-codes (MAFIA and URMEL-T) and with measurements for a simplified 36 cell structure [11]. An excellent agreement between the mode matching results [18] and MAFIA was found as well as a good accuracy of the coupled oscillator model [20].

According to the time domain calculation [9] the dominant contributions to the transverse wake are found in the frequency range between 4.1 GHz and 4.5 GHz, related to modes of the *first dipole passband*, and between 9 GHz and 10 GHz, related to modes of the *sixth dipole band*. Contributions from other passbands are intrinsically small compared with the two main bands. The behaviour of the dominant dipole bands is sumarized in Table 4.2.2.

	band 1	band 6
initial coherence	no contribution above $0.05\hat{w}$ and at multiples of the bunch distance	contribution between $0.05\hat{w}$ and $0.15\hat{w}$ for the first 8 bunches
decoherence	contribution below $0.05\hat{w}$ at the first 72 bunches	contribution below $0.05\hat{w}$ for the next 33 bunches
maximal recoherence	$\max\{\lvert w_D(s=135\,\mathrm{m})\rvert\}$ $=0.2\hat{w}$	$\max\{\lvert w_D(s=80\,\mathrm{m})\rvert\}$ $=0.07\hat{w}$

Table 4.2.2: *Contribution of the 1st and 6th passband to the normalized transversal dipole wake $w_D(s)$ at the position of following bunches $n \cdot s_{\mathrm{bunch}}$ for s_{bunch}=1.8 m (or t_{bunch}=6 nsec) in a perfect conducting structure without dampers. All values are related to the peak value $\hat{w} = \max\{\lvert w_D(s)\rvert\} = 1.64 \cdot 10^{16}$ V/(Cm). For small values of s modes of one band are coherent and may substantially contribute to the wake. As the frequency separation of the modes is approximately constant they recohere again on a longer distance (time) scale.*

Wake Field Suppression Three different cures are foreseen in the design of the accelerating structure to reduce the wake-field kick of the dominant bands below $0.05\hat{w}$, which is the peak of the wake field at t = 0, to fulfill the present requirements given

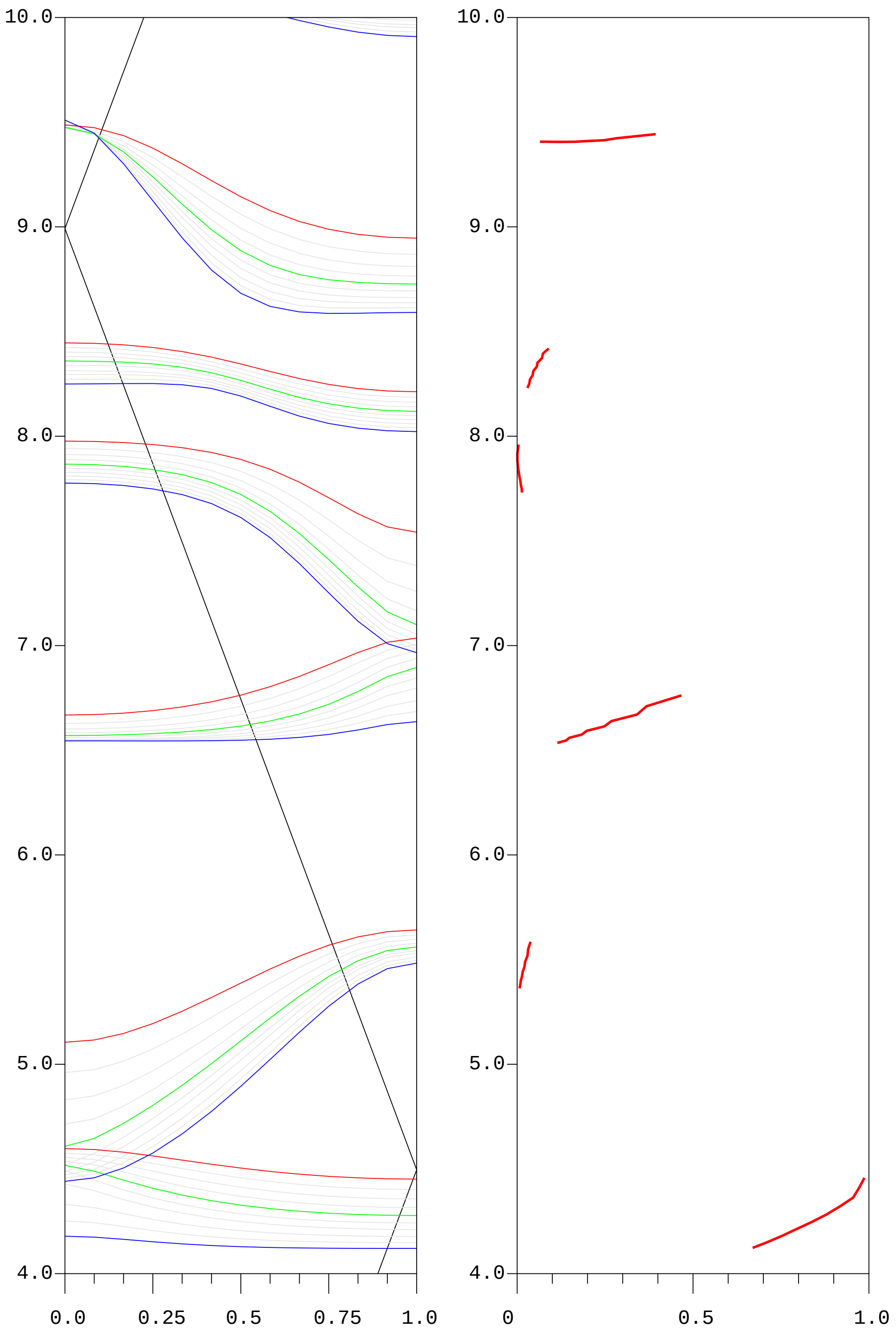

Figure 4.2.9: *Dispersion curves for the accelerating structure assuming periodic boundary conditions for the individual cells are presented in the left plot. The upper and the lower curve in each passband correspond to the first and the last cell in the structure (or vice versa). The plot on the right hand side shows the corresponding loss parameters (normalized to the strongest one) as a function of the frequency of the modes interacting with the beam.*

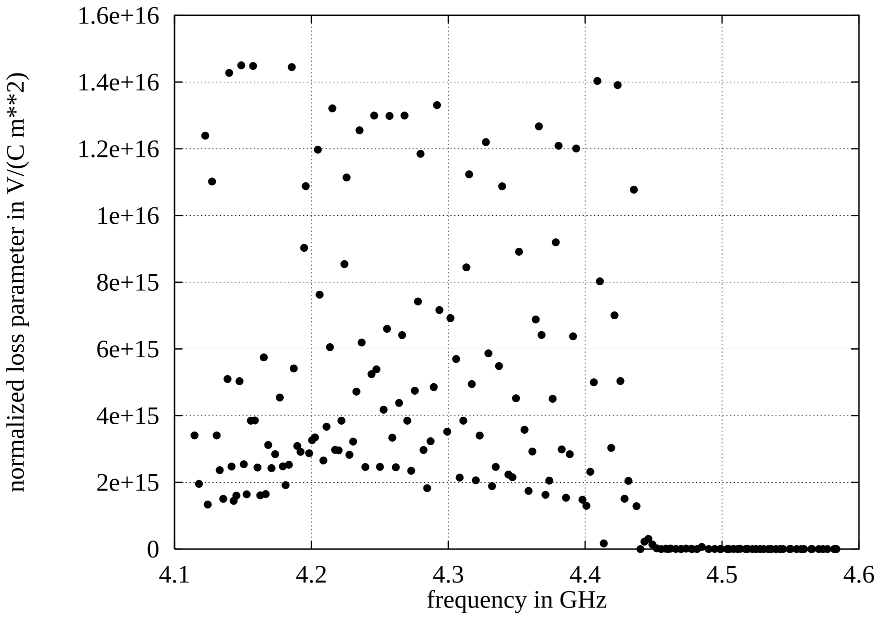

Figure 4.2.10: *Normalized longitudinal loss-parameters of a piecewise tapered 180 cell S-band structure calculated by the mode matching technique [10].The strong variation of the parameters is caused by the piecewise tapered geometry.*

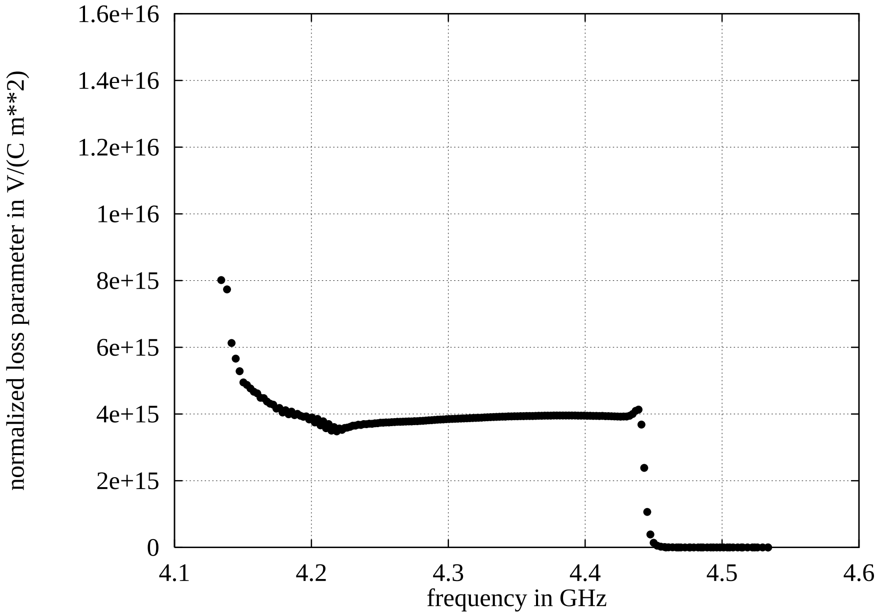

Figure 4.2.11: *Normalized longitudinal loss-parameters of the continuous tapered SBLC-structure calculated by the double-band coupled oscillator model [20]. Most of the modes with high loss-parameter are completely trapped in the disc loaded structure.*

by the current and emittance from the 500 GeV table of parameters. In addition, the potential to accelerate a significantly smaller emittance is part of the design as well.

- The first method is almost given for free, because constant gradient structures are proposed. Due to the taper of the iris which is necessary to produce a constant power loss per unit length, the structure is intrinsically *detuned* for other passbands than the band of the accelerating mode [10]. The DETUNING can be improved be variing further cell dimensions (e.g. the iris thickness) along the section [17].

- Any detuning is limited by re-coherence of these modes given by the inverse of the typical mode spacing in frequency within the passband. In our case the re-coherence length is short compared to the bunch train length. Therefore additional DAMPING of these modes is necessary.

- In order to keep the excitation intrinsically small an ACTIVE ALIGNMENT system is foreseen (compare Sect. 4.2.2) which can move the accelerating structure according to dipole mode signals extracted from higher order mode pick ups. The resolution is limited by the straightness of the structure and the sensitivity of the HOM pickup.

Detuning Cell-to-Cell Detuning In a constant gradient structure the iris diameter is tapered (decreased) from the front to the end cell to provide a constant power loss per unit length and therefore a constant (unloaded) gradient. The SBLC structure is tuned to have a constant phase velocity in the accelerating $2\pi/3$ mode at a given frequency of 3 GHz. For all other passbands the synchronous frequency changes slightly from cell to cell because of the geometry change. Therefore not only one mode per passband with n times the single cell loss factor is excited by an off axis beam, as e.g. in a constant impedance structure, but many modes of each passband contribute to the transverse kick with a loss factor of the same order of magnitude. The destructive interference of these oscillations can be used to suppress the wake-field on at time scale given by the total frequency spread and the typical frequency offset between modes.

For X-band structures it has been shown in [12, 14, 15] that the first part of the long range wake can be reduced by more than two orders of magnitude by pure detuning. Such a suppression factor is required as shown by beam dynamics calculations and can technically be achieved by modifying the group velocity profile and simultaneously tapering the iris thickness. The requirements for wake field suppression, straightness and alignment of a S-band structures are comparatively relaxed even with higher bunch charges because the transverse wake fields scales with the third power of the frequency. This is one of the strong arguments for low operation frequency.

The 'natural detuning' (constant gradient group velocity profile) provides a destructive interference for modes of the *first passband* which reduces their contribution to the wake field by more than a factor of twenty for the next seventy bunches. Beam dynamics simulations in Sect. 4.3 and [9, 16] which are based on the dipole modes of the first passband calculated in [10] have been done. They indicate that the initial decoherence reduces the wake field of the lowest band sufficiently for the first few bunches.

The time domain calculation [9] and the mode matching analysis [18] predict in good agreement, that in the *sixth passband* only very few modes in a narrow frequency interval will be excited by the beam. For this reason the spectral components between 9.45 GHz and 9.48 GHz do not decohere within a few nanoseconds and dominate the wake function for the first couple of bunches. To suppress this contribution below $0.05\hat{w}$ either strong damping ($Q < 200$) is necessary or the detuning bandwidth has to be increased to 150 MHz. For X-band structures it is been shown in [17, 15] that this can be achieved by tapering the iris thickness.

Section-to-Section Detuning Section to section detuning is a well known and proven technique to increase the multi-bunch beam breakup threshold. It has first been applied to the SLAC linac after installation. Later on this technique has artificially been introduced in many linac designs, where long current pulses are used, e.g. in low energy nuclear physics high duty cycle accelerators [19]. At SLAC three classes of structures have been provided by shifting the resonance of the first and strongest mode from the first passband at 4140 MHz by 2 MHz and 4 MHz by specifically detuning the first few cells of the accelerating structure. While for the SLAC structure the most disturbing modes are located at the front end of the three meter section, with a six meter structure more modes are completely trapped inside. In addition, with the parameters used for the S-Band collider study, the frequency spectrum of the beam exciting the structure is much denser because the bunch to bunch distance is 6 nsec as compared to 0.3 nsec (fundamental of S-Band with every bucket filled used for SLAC operation). For both reasons more modes will be excited as compared to the operation mode of the SLAC linac. In addition ten different classes of sections with a scatter in resonant frequencies for the same modes have been assumed for the beam dynamics calculations (compare Sect. 4.3). The frequency spread of the shift is ± 18 MHz shifting the frequency of each mode in the passband by the same amount. Technically this will be achieved by changing the single cell geometry and/or the group velocity taper of the structure.

Damping Damping of the wake-field is necessary on a time scale determinded by the *re-coherence* of the wake-fiel which itself is affected by detuning imperfections due to *manufacturing tolerances*. Both effects become important on a much longer time scale compared to the bunch to bunch distance. The quality factor of modes in the first passband has to be less than 4000 to prevent intolerable emittance growth caused by the re-coherence after approximately 450 ns. For this calculation a 1 MHz rms frequency error of the dipole mode resonances has been assumed. The re-coherence time of modes in the sixth band is approximately 270 ns, but due to the lower maximum wake-field after re-coherence and the higher frequency the Q has to be reduced to 8000 only.

Although very weak additional damping is required the quality reduction for modes in the first dipole band cannot easily be achieved with a few HOM dampers distributed along a section. This is due to the existence of *trapped modes* which are localized in certain parts of the tapered structure and do not have any field close to the input or output end. In the SBLC structure approximately 140 modes (in the first dipole band, for each polarization) are completely trapped. Such a trapped mode has a field distribution within 1/3 of the section with a very non-uniform energy distribution. To sufficiently couple to all the trapped modes approximately four to six pairs of higher order mode dampers would be required for each polarization. The disadvantage of this method is not only the large number of specialized cells which complicate the structure assembly, brazing and tuning but also their interference with the detuning. The different geometry of damper cells changes the frequency, amplitude and phase distribution within the structure of the beam driven modes, leads to a less perfect decoherence and consequently asks for even stronger damping. Instead we propose to intrinsically damp every cell and use loosely coupled higher order mode damper cells for HOM detection only, which change the mode patterns only weakly. The goal is to increase the surface resistivity at certain parts of the cell without decreasing the accelerating mode impedance by more than 5%, in order to damp the most harmful HOMs sufficiently [20]. By evaporating a $10\,\mu$m to $20\,\mu$m surface layer on the tip of the iris with a material of low conductivity the required damping of modes in the first and sixth band can be achieved [20, 21]. The materials which have been used are stainless steel or Kanthal and dependent on the thickness, but more on thechoice of the material, this corresponds to one or a few skin depth.

The integrated load at the end of the structure which is normally used to terminate the accelerating mode power, additionally fulfills the purpose of a higher order mode absorber for those modes which extend into the load. This does not work for the majority of modes, which are trapped apart from the load, but the other modes can be damped. For instance the modes of the sixth dipole band with a high shunt impedance extend along the whole structure length. The matching for these modes is not perfect as the local group velocity is approximately three times higher than for the accelerating mode and the the quality is about 40% higher, but the power dissipation is still substantial.

<u>HOM Damping by Intrinsic Losses</u> The damping of dipole modes in the first pass-band by increasing the surface losses in the coupling holes has been proposed in [20, 21]. In contrast to the electric cell to cell coupling of the accelerating field the lowest dipole modes essentially couple via magnetic fields and the magnetic energy distribution on the surface of the iris tips is very different (see Fig 4.2.12). The surface currents in the coupling iris are much higher for dipole modes as compared to the accelerating field. Therefore dipole modes are more sensitive to high loss material in this area. In order to reduce the quality factor of a dipole mode from 14000 to 3000 the surface resistivity in the iris holes has to be increased by a factor 15 to 20. At the same time the quality factor of the monopole mode is only reduced by about 5% .

To increase the surface losses the cavity is covered partially by a thin metallic layer (see Fig. 4.2.13) with a reduced conductivity or increased permeability. In [20] a test with sputtered layers of stainless steel and Kanthal are described. The electric properties of such a layer can be controlled in a wide range (absorption factors between 10 to 30) by the choice of material and the thickness of the layer. A third degree of

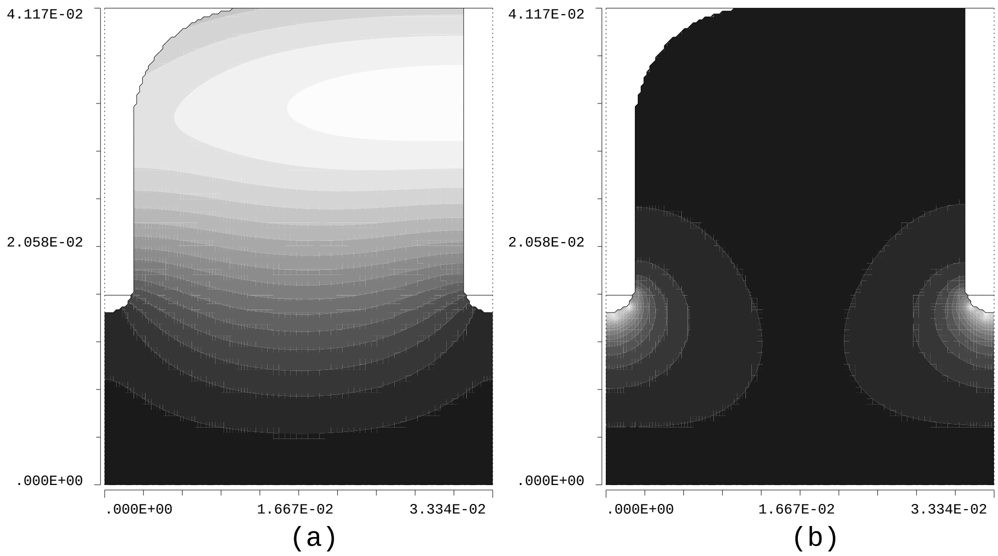

Figure 4.2.12: *Magnetic energy distribution in one cell of the SBLC structure: a) accelerating mode. b) dipole mode (first passband, $\pi/3$ traveling wave mode). The surface losses are proportional to the magnetic energy distribution at the surface. Plotted is the energy density averaged over time and azimuthal position. Low energy corresponds to dark gray.*

freedom is the height d_{coat} (see Fig. 4.2.13) of the covered surface.

The iris coating is exactly at the location with the highest electric field strength. In [21] a two cell test resonator was used for high power test. The maximum available power of 900 kW in this setup generates a $\pi/2$ standing wave field with the same iris field strength as compared to the unloaded accelerating field ($2\pi/3$) of 25 MV/m in the traveling wave structure. For the processing time and the result no difference could be found between cavities with sputtered stainless steel, sputtered Kanthal or galvanic Kanthal layers as compared to plain copper cells and no indication for extraordinary surface breakdown could be observed.

For all modes from the first passband with a high loss factor the quality factor has to be below $\mathrm{Q} = 4000$. If the power dissipation for the acclerating mode should be constant at the same time and the height $\mathrm{d_{coat}}$ (see Fig. 4.2.13 of the covered area around the iris tip does not change, the absorption factor P (P = surface resistivity with covering/ surface resistivity without covering) has to be increased approximately linear with the cell number, because the ratio of covered to uncovered area decreases along the section:

cell number	group velocity	Q reduction acc. mode	absorption factor P
1	4.06	5%	10
		10%	21
180	1.35	5%	21
		10%	43

With a constant absorption of the accelerating modes in all 180 cells, the quality

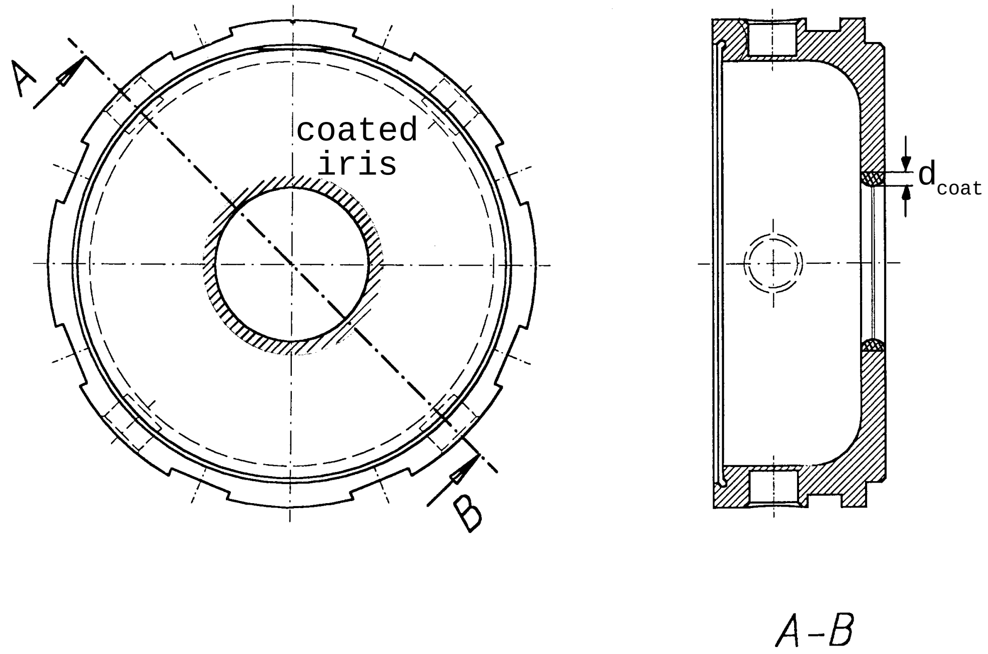

Figure 4.2.13: *Iris tip coating with a thin metallic layer.*

factors of modes in the first dipole band are shown in Fig. 4.2.14. Note that only modes below 4.45 GHz have a high HOM loss parameter as can be seen in Fig. 4.2.10 and Fig. 4.2.11.

For a constant gradient structure the fill time τ_{fill}, the damping parameter τ and the quality factor Q of the accelerating mode are related by

$$\tau_{\text{fill}} = 2 \cdot \tau \cdot Q/\omega.$$

If the fill time is kept constant the reduced quality factor allows to increase the damping parameter τ by changing the group velocity profile along the structure. Due to the higher damping parameter more of the input power P_a is available for the absorption inside of the structure $(P_a - P_b = P_a * (1 - \exp(-2\tau))$ and therefore the additional losses caused by the coating are partially compensated. Increased monopole losses of 5% and 10% as asumed for the Q-distributions in Fig. 4.2.14 reduce the average section shunt impedance only by 2.6% and 5.2% .

Active Structure Alignment The necessary components for the structure alignment are: the HOM pickup, the readout electronics and a feedback loop including the movers to position the section (compare Sect. 4.2.2). The active alignment uses single bunch operation because even small misalignments upstream would cause deflections of following bunches so that the beam axis is not unique and the resolution of the measurement is decreased. This effect would accumulate for structures downstream.

The structure alignment should not be limited by the sensitivity of the beam offset measurement and provide the potential of accelerating and maintaining a factor of two to three smaller emittance beams. Therefore the goal for the resolution is 10 μm

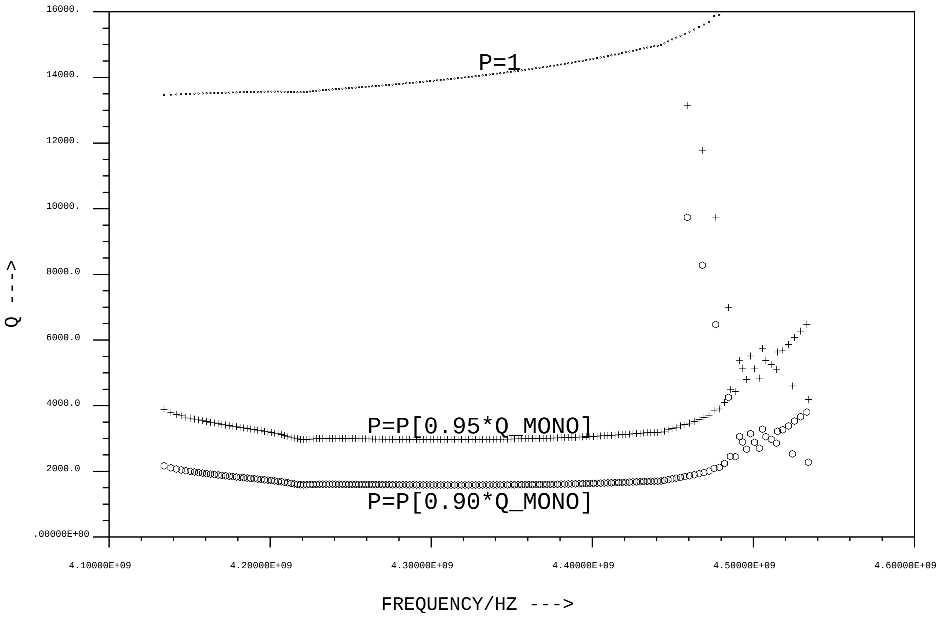

Figure 4.2.14: *Quality factors of the first 180 dipole modes in the tapered SBLC structure without iris coating and with length dependent coating. The surface absorption coefficient P is set for every cell so that the absorption of the accelerating mode is increased in every cell by 5% and 10% ($d_{\rm coat}$=1.5mm). The quality for modes with high loss-parameter ($f < 4.45$ GHz) is significantly reduced. Some modes above 4.46 GHz have a qualitatively different field pattern and q factor due to a coupling to the second band in some cells.*

whereas only 50 μm is required for the 500 GeV parameters. With the offset of 10 μm a single bunch with design population (1.1×10^{10} particles) deposits approximately $1.3{\times}10^{-12}$ joule in each of the 140 dipole modes of the first passband. Due to iris coating (leading to a Q of 3000) the energy decays with a time constant of 0.22 μsec which corresponds to a power flow of about 5 μW per mode. Only a fraction of this amount can be extracted by a HOM pickup which is designed for small change of the cell to cell detuning. The signal diagnostics can either lock to a particular mode with a bandwidth determined by its decay time constant (approximately 1.5 MHz) or it can use the full pickup bandwidth which is approximately half the width of the passband of the coupler cell ($\approx$ 0.5*100 MHz). Only a fraction of the modes within the pickup bandwidth provide sufficient coupling so that only 10 to 20 resonances are observable. In contrast to the small signal level of dipole modes, the power flow of the accelerating mode is more than ten orders of magnitude larger. One way to improve this situation is to switch off the klystron power of the section to be aligned, but beam loading still creates significant field levels towards the end of the section. On the other hand, mode or frequency selective equipment can provide sufficient performance.

HOM Coupler For every SBLC section two HOM pickups with four orthogonal waveguides at one cell are foreseen. Two opposite waveguides are used for one polarization plane. The pre-selection is given by the cutoff frequency of the waveguide. After coupling to a TEM transmission line bandstop filters reject the accelerating mode and hybrids are used to distinguish between symmetry and anti symmetry of monopole and dipole signals.

The HOM coupler shown in Fig. 4.2.15 uses azimuthal wall slots for coupling [22]. The slots and the rectangular waveguides are 37.5 mm in width and thus have a cutoff frequency of 4 GHz. The acceleration mode at 3 GHz, which is well below the cutoff frequency, decays exponentially along the waveguide. The HOMs are above the cutoff frequency. For good rejection of the accelerating mode, the pickup (for the signal) is

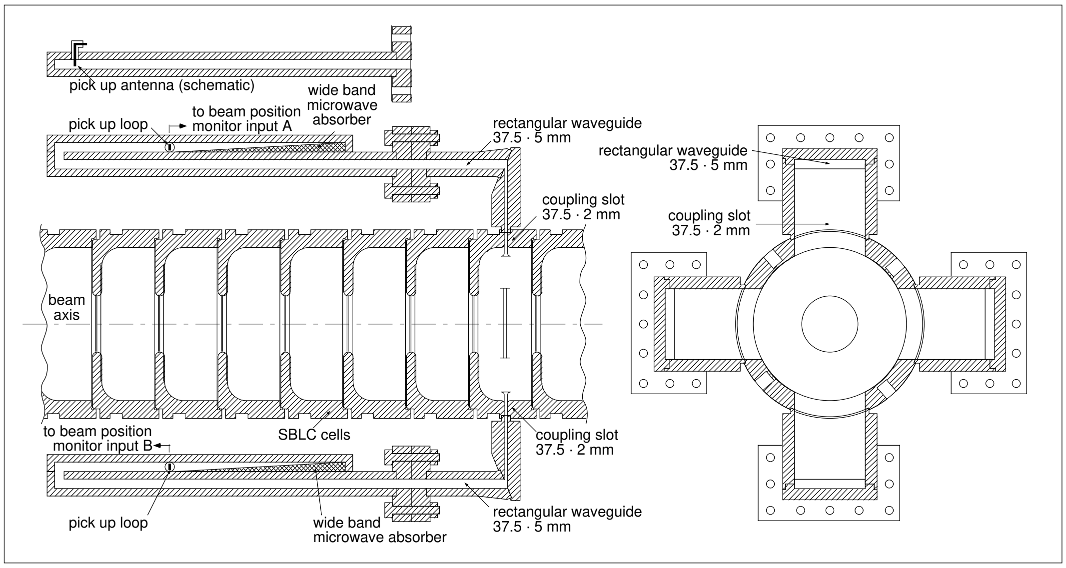

Figure 4.2.15: *Cross sectional view of the accelerator structure with one HOM-coupler*

mounted as far as possible away from the slot. Fig. 4.2.15 shows two alternative designs for the waveguide behind the flange. The upper illustration shows a straight waveguide with a pick up antenna mounted with a vacuum sealed connector. The length is limited by the free space which is left by the structure support. The other option which is also shown in Fig. 4.2.15 is a folded waveguide with wide band microwave absorber material at the end of thus waveguide. The pick up is realized by a wire loop mounted on a vacuum sealed connector at the side of the waveguide. This option has a better rejection for the accelerating mode and avoids disturbing standing waves, which influences the measurement. The disadvantage is a higher price and a more complicated fabrication.

A more compact solution with only one coupler is possible by coupling to modes of the sixth passband which are not trapped. Due to the high frequency of 9.4 GHz the coupling geometry and waveguides need only the half size and the frequency separation to the fundamental mode is wider.

Signal Processing for Active Structure Alignment To detect both sign and magnitude of a transversal beam displacement the signal processing electronic needs signals from a TM-like dipole mode at about 4.3 GHz and a monopole mode at 6.2 GHz [23]. The accelerating monopole mode is not suitable for this purpose, because it does not propagate through the waveguide and has an amplitude which is not proportional to the beam current. The usage of a higher order monopol mode makes it possible to measure the beam position without klystron power. The magnitude information is derived from a dipole mode amplitude whereas the sign follows from phase comparison of a dipole and a monopole HOM during the time of bunch passage. Both signals are taken from the pair of pickups at the waveguide HOM-couplers. Figure 4.2.16 shows a possible scheme to process the signals from the coaxial pick-ups for one direction. The first stage is a 180° ring hybrid. The dipole signals from the HOM couplers have

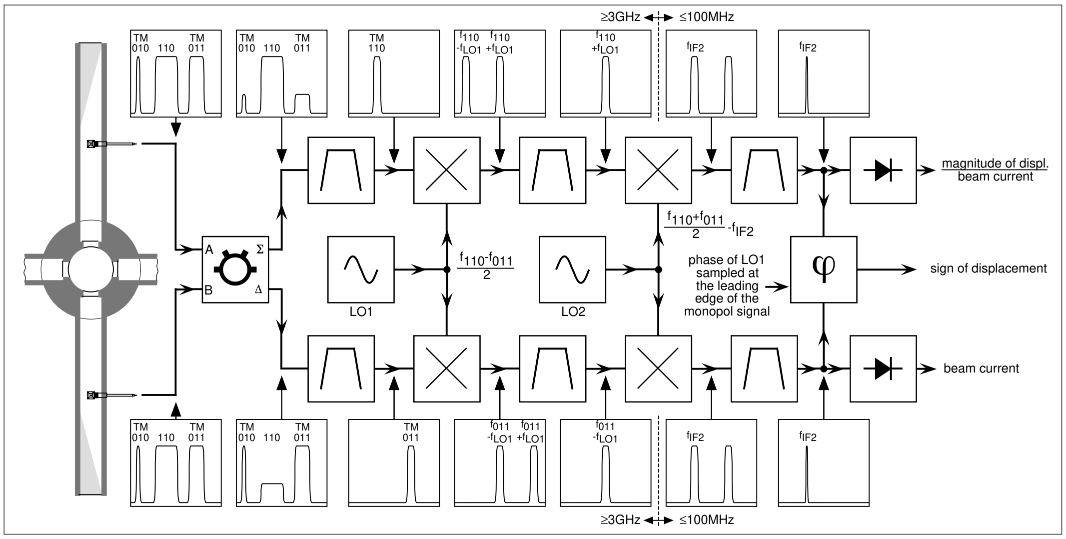

Figure 4.2.16: *Signal processing scheme for beam position monitoring in one direction (developed at IAP Frankfurt [23]) using HOM coupler signals*

same phases at the two pick-ups, which are mounted in opposite direction, thus the signals are transmitted to the Σ-port. The monopole signals have opposite phases and thus they are transmitted to the Δ-port. The hybrid is designed to reject monopole signals from the Σ-port which occur at the frequency of the dipole mode due to the finite Q of the cavities. The ring hybrid has to be mounted near by the couplers to avoid unsymmetrical phase shifting and damping by long transmission lines.

The first pair of filters consists of micro strip-line resonators with a bandwidth of about 50 MHz. It rejects modes of wrong passbands. A filter with a small bandwidth at this position has the disadvantage that it becomes impossible to tune the monitor to a different mode. Further the phase shift due to the temperature drift of the filter becomes too large. The filter block includes also variable amplifiers for the adaption to different operating situations. For fine tuning or pilot bunches one needs higher amplification than for coarse adjustment and full current bunch trains. The first local oscillator is tuned to one half of the frequency difference of the dipole and the monopole mode. With this frequency the monopole signal is mixed downwards and the dipole signal is mixed upwards to the common frequency:

$$\omega_{IF1} = \frac{\omega_{mono} + \omega_{dipol}}{2}$$

The common frequency is needed for the phase comparison behind the second mixer. The filter behind the mixers selects the correct side band of the mixer signal. The second mixer stage mixes both signals downwards to a frequency of 70 MHz for the final filtering.

So far all components are micro strip-line circuits. This allows to integrate the ring hybrid, the filters and the phase shifters inside the mixers as line structures on a single PTFE printed circuit board. The following lower frequency components are lumped circuits on an unmatched printed circuit board.

Both quartz SAW filters have a narrow bandwidth and separate a single mode of each signal. The following rectifiers and low pass filters extract the amplitude of the signals. The magnitude of displacement and the beam current is determined by these two signals. The phase difference between the two second intermediate frequency signals is measured by the complex mixer between both paths. Due to the scheme of the first mixer pair (up-/down-mixing) the phase difference between the monopole and the dipole signal cannot determined only by measuring the phase difference of the second intermediate frequency (IF2) signals. The signals are given by:

$$u_{IF2mono} \propto u_{mono} \cdot \cos(\omega_{IF2} t + \phi_{LO1} + \phi_{LO2})$$

$$u_{IF2dipole} \propto u_{dipole} \cdot \cos(\omega_{IF2} t + \phi_{dipole/mono} - \phi_{LO1} + \phi_{LO2})$$

The measured phase difference depends on the phase of the first local oscillator at the time of the bunch passage. To get this phase we detect the leading edge of the monopole signal. A diode rectifies the envelope of the signal. This is done at a position with broad bandwidth, so we have a sharp rising edge. From the envelope a clipping line pulse former produces a short pulse to drive a dual sampling bridge sampling the complex signal of the first local oscillator to allow the determination of its phase at the time of the bunch passage.

After the A/D-conversion of all resulting signals a microprocessor does the non real time signal processing and the control and regulation of the local oscillator frequencies and amplifications. A frequency offset of the first local oscillator results in linear ramps instead of a constant signal for the phase. The frequency of this ramps is equal to the offset. A frequency offset of the second local oscillator results in an offset of the second intermediate frequency.

The information about the displacement and the beam current will be transmitted digitally from the microprocessor to the position control system of the structures.

4.2.2 The Support Structure

The approximately 6 m long accelerating structure has seven support points, spaced 933.8 mm apart, resting on a tubular steel girder (called "tube"). The tube is mounted on four remote controlled micro movers which are fastened via course adjustment units to the concrete floor. The cross section and a side view is shown in Fig. 4.2.17. At the first support the rf-structure is fixed to the tube, while at the six other supports it rests on adjustable pairs of rolls. Therefore the structure is aligned transversely but longitudinal motion due to thermal expansion is still possible.

The distance of $\approx$940 mm between structure supports is a compromise between the minimum number of supports and the natural sag. The tolerance given for straightness is $\leq 50\,\mu$m rms while the calculated sag for the given set-up is $3\,\mu$m only. The supports are adjusted with respect to an ideal line and the structure is fixed by its own weight. Deviations from this axis with a wavelength shorter than the support distance can of course not be corrected this way (compare: Material Preparation and Assembly).

Thermal effects which disturb the straightness of the support tube dominate the transverse displacements once the rf structure is aligned on top. These effects have been investigated in detail with the FEM code ANSYS. The steady state heat distribution and the time dependent behavior for heat-up are of main interest. The relevant parts of the somewhat simplified system which has been used in the model are the rf-structure as a linear heat source at a constant temperature of 75°, which is the foreseen operating temperature, together with the supports connected to the tube and the tube itself. Radiation into the environment (e.g. tunnel air at 20 deg C) and heat flow into the support structure has been taken into account. In the 2 D model the components are considered to be infinitely long. The final geometry consists of an inner support tube made from stainless steel and two outer heat shields made from aluminum. In between Styrofoam layers are used for isolation.

One main influence is given by conduction via metal parts. Heat flows from the rf-structure via the supports through the mechanically stable and thermally resistant INVAR tube downwards to the center. These tubes are fixed like spokes into the main tube with a diameter 457×6.3 mm. The "spoke"-tube equally splits the heat flow to enter the main support symmetrically (Fig. 4.2.17). Heat then flows mainly in the direction of the tube axis. A heat sink is given by the tunnel floor. Only temperature distributions symmetrical with respect to vertical and horizontal mid-planes of the tube result, They will locally set up mechanical stresses in the tube but, because they are symmetrical as well, cannot produce bending deformation.

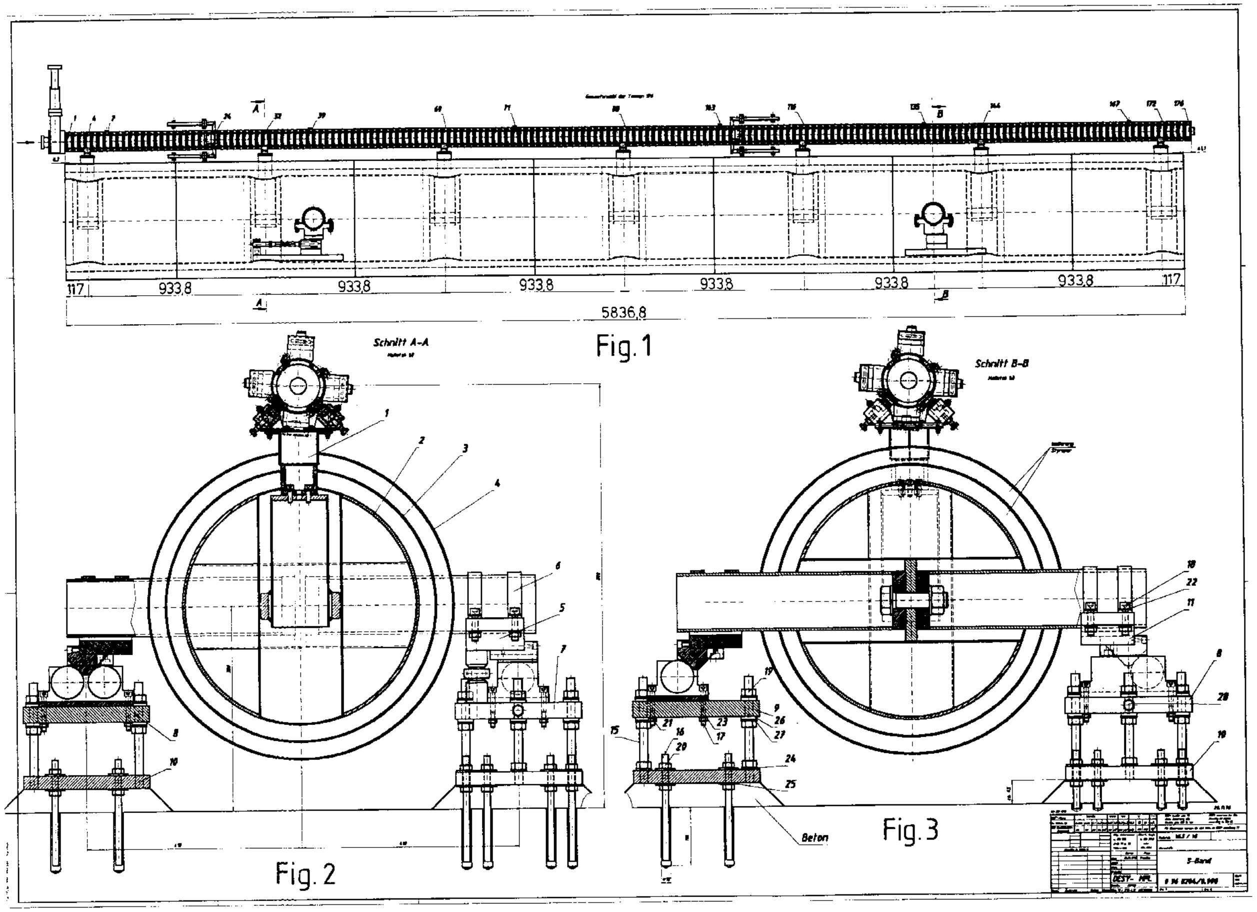

Figure 4.2.17: *The support structure together with the six meter long accelerating structure and two cross sectional views (front end and back end) is shown. Seven supports for the accelerating structure on top of the support tube can be seen. Vertical and horizontal support tubes inside the main six meter long support tube are shown as well. These "spoke"-tubes are at every support point. Close to the front end and at the back end the micro movers as well as the HOM mode pick up stations on the structure are shown.*

The second main distortion is given by heat radiating from the rf-structure and heat conduction via air. The power coupled into the outer Al-shield tube flows through the shield wall to the bottom and continues to the tunnel floor. In Fig. 4.2.18, for steady state conditions, the larger heat conductivity of the shield tube together with the comparatively lower heat conductivity between tube and heat source as well as tube and tunnel floor results in a low temperature difference of 1.32K between the top and the bottom of the outer shield. Only a very small fraction of total heat flow will enter

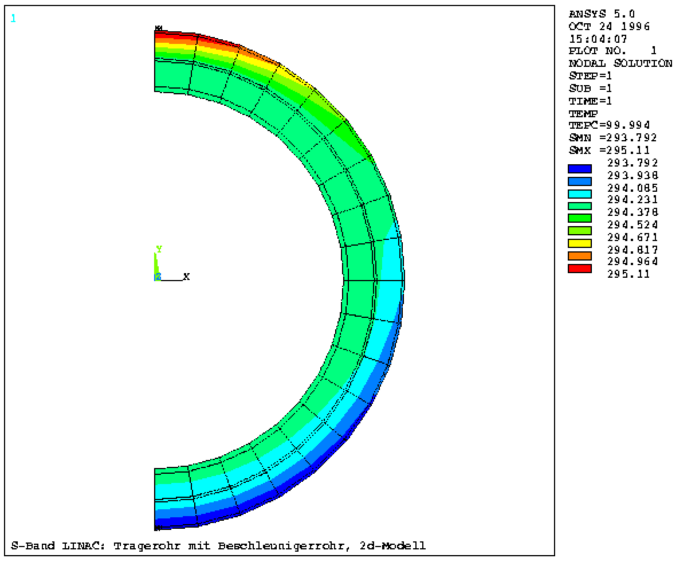

Figure 4.2.18: *The steady state temperature in one half of the support geometry is shown. The heat source is on top.*

through the outer Styrofoam layer to the inner shield. This results in a temperature difference over the shield of $\Delta T = 0.11\,K$ from top to bottom. By the same principle the main tube (made from iron) will have a temperature difference of $\Delta T = 0.013\,K$ from which a sagitta of only $2\,\mu$m results. This value is much lower compared to the initial goal of $10\,\mu$m and - after verification in the S-Band Test Facility - simplifications can be considered. in addition time dependent calculations show that due to the Styrofoam isolation the thermal response is very slow. In Fig. 4.2.19 the steady state and the temperature distribution after 72 hours is shown. Still a difference can be seen. Due to the slow thermal response fast temperature changes will be decoupled from the motion of the support.

Vibration, another very important aspect for the design of the support structure,

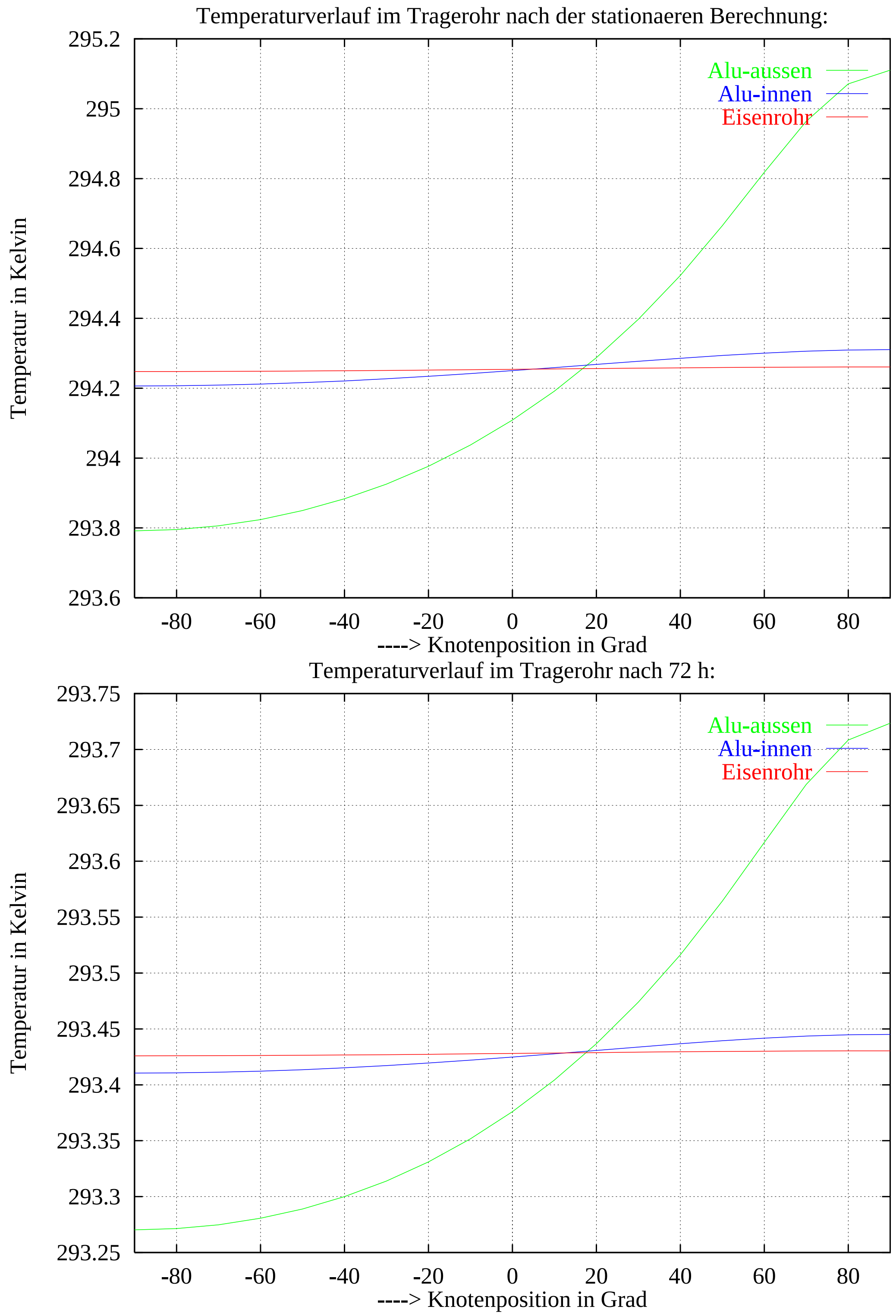

Figure 4.2.19: *The steady state temperature distribution (top) and the temperature distribution after 72 hours (bottom) of the two outer aluminum tubes and the inner iron support tube is shown. A linear heat source on top (75 C°) of the support structure and a 20 C° floor is assumed for the calculation. The temperature is shown versus the angle measured from the bottom (-90°). The calculation demonstrates the demonstrates the thermal inertia of the support structure.*

has been investigated as well. The lowest resonant frequencies for the tube is 35 Hz for any vertical flexure. Resonant modes close to 50 Hz or multiples have been avoided.

4.2.3 Alignment and Movers

The optimum orbit in the linear collider is determined by the magnetic axis of the focusing quadrupoles. Once this orbit has been achieved, the electric center of each accelerating structure has to be aligned with respect to this orbit. This will be achieved by minimizing the higher order mode power coupled by the beam into the dipole modes of the section. Therefore the position of the accelerating structure has to be changed and periodically adjusted during operation. Any transverse motion can be done by a system similar to that used for moving the focusing magnets in the Final Focus Test Beam[24] at SLAC. Cams are driven in phase via step motors to adjust the position to about $\pm 10\mu$m relative to the the beam. Some technical details of the the solution chosen for the S-Band Test Facility are given in Table 4.2.3.

As illustrated in Fig. 4.2.17, each section will be mounted on two micro-mover units, supporting two points at each end. The micro-mover unit at one end will have three drive motors and the one at the other end two, giving altogether five motors for motion with five degrees of freedom. Any long term motion ($\geq \approx$1 minute) thermal or tectonic up to ± 1.5 mm will be compensated using this technique.

Table 4.2.3: *Micro-mover specifications*

Parameter/Item	Specification
Principle of movement	Cams phase-driven via step motors
Cavity section: Weight Length	 1000 kg 6 m
Positioning per section	
Two micro-mover units:	Front end unit á 3 motors Back end unit á 2 motors
Cam Radius/offset	40mm/1.6mm
Maximum range: Horizontal Vertical	 ± 2.2 mm ± 1.6 mm
Overall ratio of transmission system	400:1
Step size of the positioning system	Minimum $< 0.3\mu$m
Tolerances	
achieved positioning precision: Horizontal Vertical	 $\sigma_{rms} < \pm 8\mu$m $\sigma_{rms} < \pm 10\mu$m

4.2.4 Temperature Stabilization

An important issue for the operation of a Linear Collider with heavy beam loading is the temperature stability of the accelerating structure. Simultaneously the flexibility to handle large variations in beam loading and average power dissipation is required. The heat source is the rf dissipated in the walls given by the difference of the total input power and the power extracted by the beam. This power is calculated from the vector sum of the accelerating voltage and the beam induced voltage, taking the shunt impedance and the attenuation per unit length as well as the repetition rate and the rf pulse length into account. The temperature variations along the structure lead to energy variations of the beam, which are given by the phase error per cell integrated along the accelerating section. The single cell phase error is determined by the frequency change due to thermal expansion and the group velocity of the cell. This value is calculated from an average temperature change at each cell with respect to a constant temperature, where the beam is assumed to be in phase with the rf wave.

The structure is geometrically tapered to achieve a constant power loss per unit length for no beam loading. Overall four cooling tubes are soft soldered on the surface of the structure. The water feed and outlet is only at the input end and there is "u-shaped" flow (forward and backward flow with short connectors at the end) over the structure length. In order to calculate the exact temperature distribution, one fourth of the total geometry is modeled. The incoming cold water is going downstream, has a return loop over the last cell and flows upstream to the outlet while constantly heating up and reaching the maximum temperature at the outlet.

For the calculation the following assumptions have been made:

- because of the symmetry only one quarter of the geometry is calculated
- the temperature gradient over the wall with a thickness of 1 cm has been neglected
- the detailed temperature distribution inside the cell has been neglected
- the water inlet and outlet are on the same end as the input coupler with counter flow in the tubes
- brazed onto the first and the last cell are a return loop (last cell) and a feed pipe (first cell)

shown in Fig. 4.2.20 in a 3-D plot assuming a beam current of 300 mA. The temperature is shown as a function of the azimuthal position between 0 and $\approx$ 8 cm and the longitudinal position between the input coupler and the structure end. Fig. 4.2.21 shows the average temperature between the cooling tubes for different beam loading conditions. This is calculated as the arithmetic average over the azimuth between the two cooling tubes at each position along the structure length.

The temperature at the surface rises continuously along the length of the structure in absence of beam current. With increasing beam current the power which is dissipated along the structure decreases, because the beam induced field is small in the first cell and maximum at the end. Therefore the heat flow into the water is lower at the end of

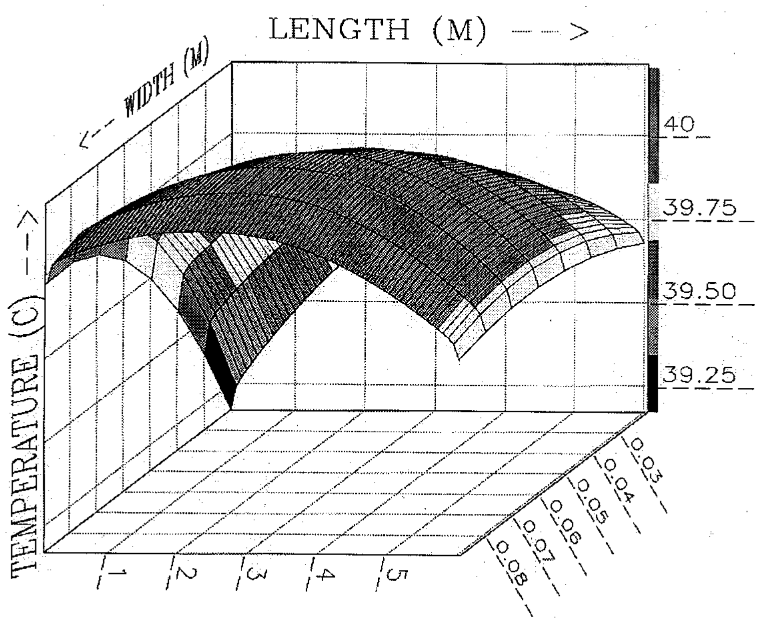

Figure 4.2.20: *Distribution of the surface temperature with a beam current of 300 mA. One quarter of the structure geometry is used for the simulation of the heat transport. Shown is the surface between two cooling tubes over the total structure length of 6 meter. The (cold) water inlet shows the lowest temperature while the temperature rises following the outer boundary of the displayed surface until the water outlet (hot) is reached.*

the structure than at the beginning. Because the heat flow from the structure surface to the water is a function of the temperature difference between them, the surface temperature increases at first and then decreases along the length with increasing currents. This effect is more pronounced with increasing beam current. The strong gradients on both ends are produced by the heat flow into the return tubes.

The integrated phase error turns into a beam energy error along the structure length. A minimum energy error can always be achieved, if the integrated phase error cancels towards the end of the structure. Using the inlet water temperature as a parameter, the phase error is zero if negative phase deviations with respect to the 120° phase shift per cell cancel with positive deviations towards the structure end. Calculation shows that at a specific point the temperature remains constant independent of the dissipated rf power or beam loading conditions. This point is used for temperature regulation and phase error compensation [26]. This location of this point is shown in Fig. 4.2.22, given by the cross-over of the curves .

For the details of the technical realization of the water cooling system see section 4.10. A similar system has been operated very successfully for many years in a high duty cycle electron linac for nuclear physics [27], where sudden power changes of more than a factor of hundred have been handled.

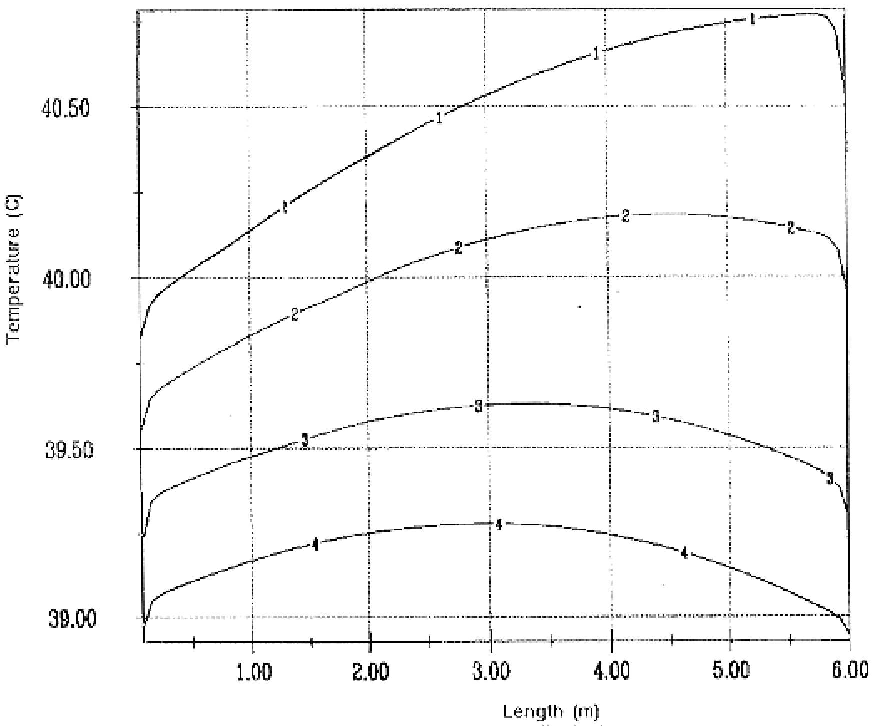

Figure 4.2.21: *Distribution of the surface temperature averaged over the azimuth for different beam loading conditions: curve 1 : no beam; curve 2 : beam current 100 mA; curve 3 : beam current 200 mA; curve 4 : beam current 300 mA. In this case the inlet water temperature was kept constant.*

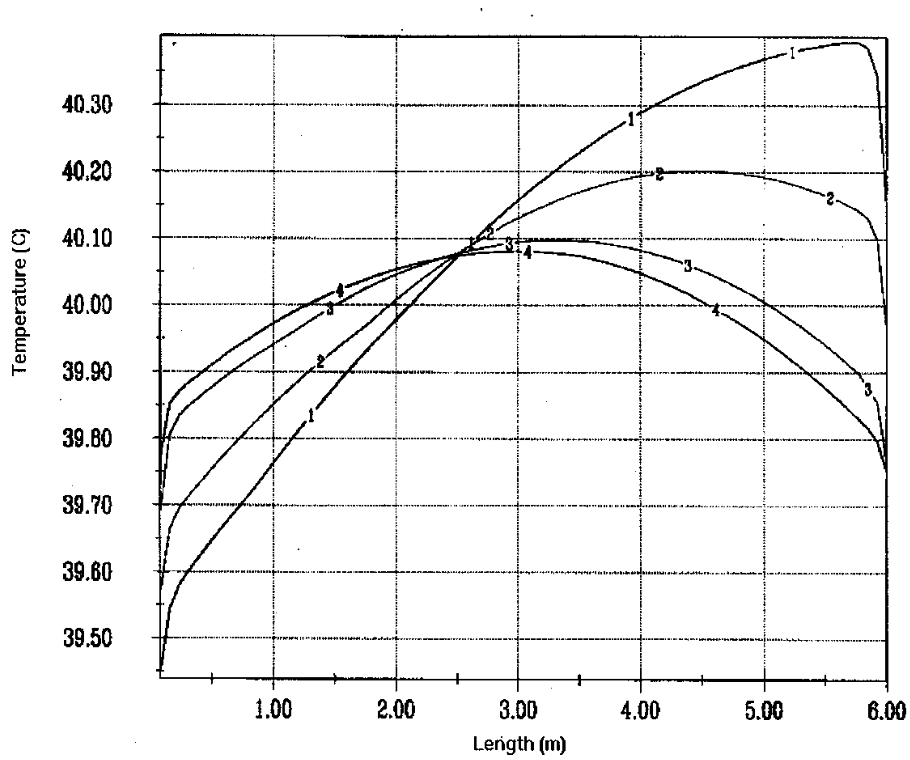

Figure 4.2.22: *Surface temperature with optimized inlet water temperature in order to cancel the sum of the single cell phase error towards the end of the structure: curve 1 : no beam; curve 2 : beam current 100 mA; curve 3 : beam current 200 mA; curve 4 : beam current 300 mA.*

4.2.5 Material Preparation, Assembly and Vacuum System Set-Up

The vacuum system of the main linac is dominated by the accelerating structure with a filling factor of more than 90 %. The achievable vacuum in the beam line is therefore given by the residual outgassing rate of the section under high power conditions. The achievable vacuum pressure in those structures is dominated by H and H_2 and is in the range of $10^{-9} - 5 \times 10^{-10}$ mbar. At the same time the required time for processing is reduced and the breakdown threshold increases.

Each accelerating section is connected to two vacuum pumps which are placed close to the input coupler. Nevertheless, the combined conductance of the beam pipe is determined by the average iris diameter, which is 26 mm. Assuming a residual outgassing rate of $10^{-8}\,\frac{\text{torr lit}}{\text{m}^2\,\text{sec}}$ which can only be achieved with carefully cleaned and assembled structures, the conductance of the six meter section limits the average pressure to approximately 2×10^{-8} Torr. Two pumps are installed next to the high power input coupler. At the coupler the main source of breakdown can be expected and optimum pumping should be applied. One pump is connected to the rectangular waveguide on top of the coupler and the second pump is directly connected to the coupler cell. Given the average pressure in the beam line and a base pressure at the pump which is ten times smaller, the installed pumping speed should be approximately 40 lit/sec per section.

4.2.6 The Radio-frequency-System

The radio-frequency system provides the rf peak power for the linear accelerator by converting ac-power to rf power. This, of course, has to be done in the most efficient possible manner. Apart fromt the fact that a lot of industrial experience exists for S-Band klystrons, again lower frequencies are favourable because the peak power, which could in principle be extracted from a single source, scales with (f^{-2}) [4]. Independent of frequency, in order to achieve the highest possible efficiency, a low micro- perveance is required. At a fixed peak power, this increases the required beam voltage. The feasible limit today on the high voltage, which we think is around 600 kV, certainly represents one limit for this value. Together with the specified efficiency this almost determines the maximum peak power which can be extracted from one klystron station.

The modulator consists of two main parts. The AC line to DC converter and the energy storage device together with the pulse transformer. The modulator has to convert the AC line power to DC pulsed power for the klystron which is already the first stage where efficiency plays a dominant role. Classical systems with power supplies and charging chokes (to double the voltage) are not efficient enough to be used in the linear collider. New types of power supplies, which are used to directly charge the energy storage device exist but have to be tested at the test facility. The energy storage device, which is a classical Pulse Forming Network (PFN) in our case, has to provide the energy per klystron pulse. Long RF pulses, which reduce the relative portion of the pulse which is lost during rise and fall time, require more storage capacity of the PFN. Economic arguments set an upper boundary, because the investment costs increase with an increasing number of capacitors, which is one of the cost driving items of a modulator. This argument also limits in some sense the frequency choice towards the lower end, because the energy which must be stored per pulse increases ($\approx f^{-7/2}$) poportional to the filling time of the accelerating structure and following the scalling law for the klystron which has been discussed before.

4.2.6.1 The Klystron

One of the strongest reasons for choosing S-Band to be the most favorable frequency for a linear collider design, is the klystron. S-Band klystrons are industrially manufactured at many places in the world and a tremendous experience is available, especially from the continuous operation of more than 240 tubes at the SLAC linac [28]. Both arguments present a strong bases for the R & D required for the power sources of such a large linear accelerator, where the highest peak power possible per station should be used. This way the number of klystrons per linac can be reduced, which contributes to cost saving since the cost per klystron does not increase proportional to the peak power.

The S-Band linear collider requires approximately 2600 klystrons operating at an output power of 150 MW, a pulse duration of 2.8 μs and repetition rate of 50 upgradable

[4] f:=frequency; This is simply given by the maximum beam current which can be extracted from the gun area, at a given reasonable limit for the current density, in a otherwise geometrically scaled klystron.

to 100 Hz. The efficiency must reach 55 % to limit the total AC power. The power required for focusing must be minimized, or even better, period permanent magnet (PPM) focusing should be used. Nevertheless it should be pointed out, that the S-Band linear collider could be operated with solenoid focusing at the expense of power which would increase by approximately 18 %. The life time of the klystrons should be of the order of 50.000 hours, which requires a robust design with a minimized number of critical components. Still on average, approximately every 20 hours a klystron will have to be changed during operation and while the accelerator is running.

The following pages present the status of the development of 150 MW S-Band klystrons. Then further necessary developments which will lead to a klystron meeting the specifications of a klystron for an S-Band linear collider will be discussed.

Until 1985 the klystron producing the highest output power at S-Band frequencies was the 5045 klystron at SLAC. It operates at a peak power of 65 MW with a pulse width of 3.5 μs and a repetition rate up to 180 Hz [29]. In 1985 a 150 MW S-Band klystron was developed at SLAC. It produced a power of 150 MW, but at a shorter pulse width of only 1 μs and a repetition rate of 40 Hz at full peak power [30]. Following this development it was anticipated that a 150 MW Klystron with 3 μsec pulse length and 50 Hz repetition rate is a reasonable R & D goal which can be achieved in few years. In 1993 a collaboration between SLAC, DESY, Philips and the Technical University of Darmstadt started to develop this S-Band klystron and the first one was successfully tested in 1994, only $1\frac{1}{2}$ years later. Until 1995 two klystrons have been built and successfully tested [31][32]. Table 4.2.4 presents the design and the achieved parameters of the klystron.

	Design	Tube 1	Tube 2
Power Out	150 MW	153 MW	150 MW
Pulse Duration	3 μs	3 μs	3 μs
Repetition Rate	60 Hz	60 Hz	60 Hz
Average Power	27 kW	27.5 kW	27 kW
Beam Voltage	535 kV	527 kV	508 kV
Beam Current	700 A	680 A	652 A
Perveance	1.79×10^{-6} A/V$^{3/2}$	1.78×10^{-6} A/V$^{3/2}$	1.80×10^{-6} A/V$^{3/2}$
Efficiency	40 %	43 %	45 %
Gain	50 dB min	56 dB	57 dB

Table 4.2.4: *Design and measured parameters of the 150 MW klystrons for the S-Band test facility*

Both klystrons, tube 1 and 2, will be used at the S-Band test facility at DESY. The first tube is already in operation. Figure 4.2.23 shows tube 1. The total height is

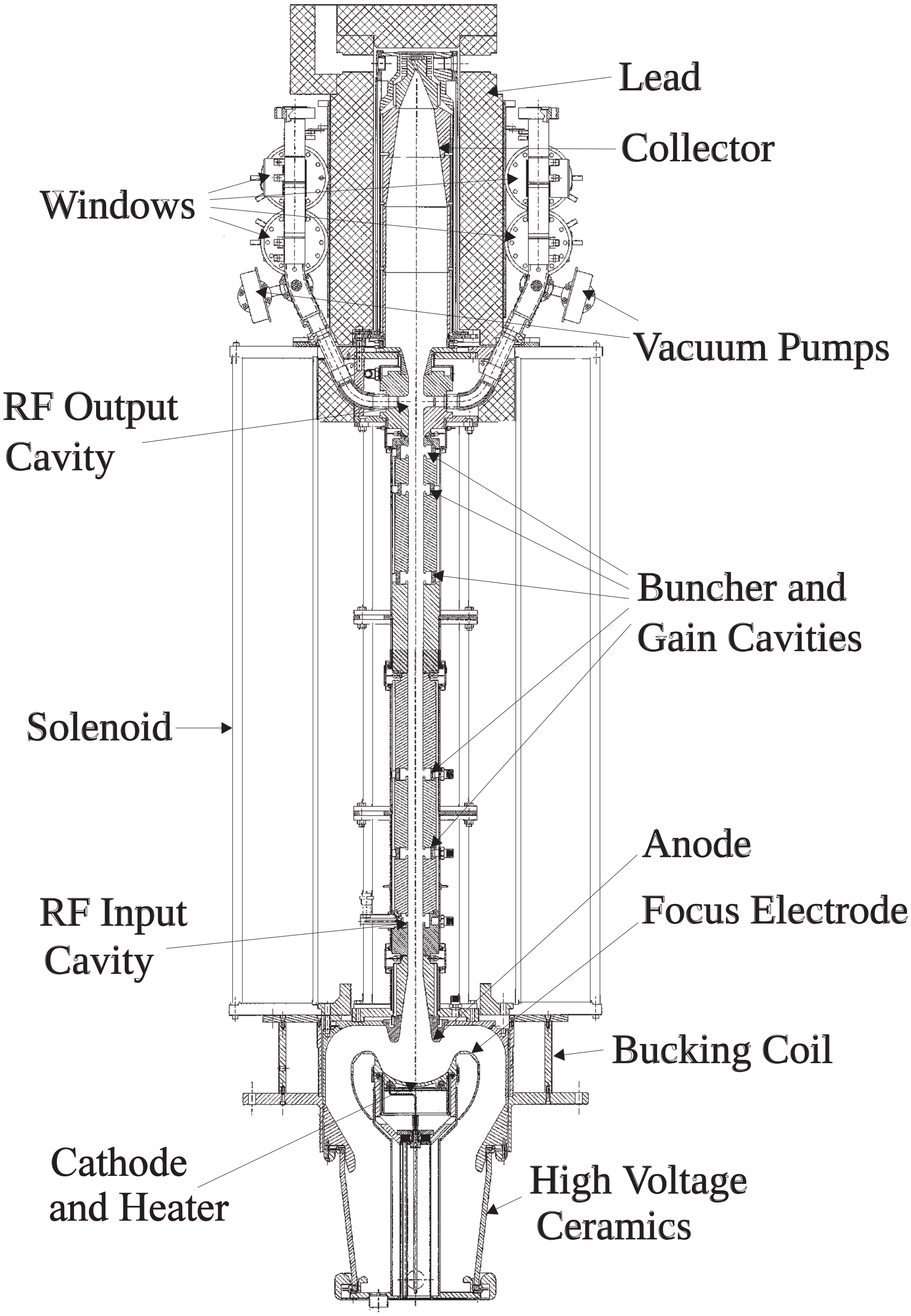

Figure 4.2.23: *150 MW S-Band klystron for the S-Band test facility (Klystron 1)*

2.6 m, the diameter of the anode housing is 40 cm and the weight is about 300 kg without lead. The cathode has a diameter of 13.3 cm and a cathode loading of 6.12 A/cm^2. The beam area convergence is 40:1. The maximum electric fields on the focus electrode and anode are 180 kV/cm and 210 kV/cm, respectively. Seven cavities including the input and output cavities are in the 3.2 cm wide drift tube.

The klystron has two output waveguides, which are split and recombined, with two RF windows in each output waveguide. The waveguide assembly on each side is the well proven design of the 5045 klystron. The klystron requires a solenoid with a magnetic field of 1800 G which has a power consumption of 14 kW. The weight of the solenoid is 1800 kg. A bucking coil is required to achieve zero magnetic field on the cathode surface.

Although both tubes are very similar in general, there are three differences between the two tubes. Already at the design stage it was decided to use different output cavities for them. Tube 1 operates with one single cavity whereas tube 2 has two coupled cavities at the output. The expectation was, that the second tube would have a slightly better efficiency compared to the first tube. As presented in Table 4.2.4, this has been achieved. During the test of tube 1 an oscillation at 8.1 GHz was observed depending on the beam voltage and solenoid field settings and in a less sensitive way on the filament power. Therefore it was decided to fabricate tube 2 with a stainless steel drift tube between the cavities 3 and 4, and 4 and 5 instead of using only copper for the drift tube as for klystron 1. This provided additional losses to the disturbing modes. The cathode was changed to a scandate cathode for tube 2, whereas tube 1 uses an osmium coated M-type cathode. The M-type cathode is known to have a distinct roll-off for the beam current versus filament power curve. Scandate cathodes have a softer transition while going from the temperature to the space charge limited regime. This allows to operate tube 2 over a wider range of filament power settings compared to tube 1. These measures have been proven very successful. No oscillations were observed during the tests with tube 2.

Figure 4.2.24 shows the output power versus drive power for different beam voltages for klystron 1. At about 400 W of drive power the output starts to saturate. Similar data exist for tube 2.

Although the development of the first two 150 MW klystrons for the S-Band collider was very successful, further R & D is required. The first two tubes have been constructed in a conservative way by using as much of proven sub-assemblies as possible. In order to increase the efficiency and to built a robust, simpler and cost effective klystron a number of changes are required.

The klystrons for the test facility are mounted vertically, but for a klystron to be used in a linear collider tunnel a horizontal mounting position is required to save tunnel space. For that reason the klystron must be stiffened and especially the klystron gun and the cathode assembly must be supported.

Each of the four windows in the two output waveguides represents a possible source for klystron failure. Instead of using two windows per output waveguide by splitting and recombining one could use one window without splitting the waveguide. This reduces the number of windows to two in total and might reduce the number of window

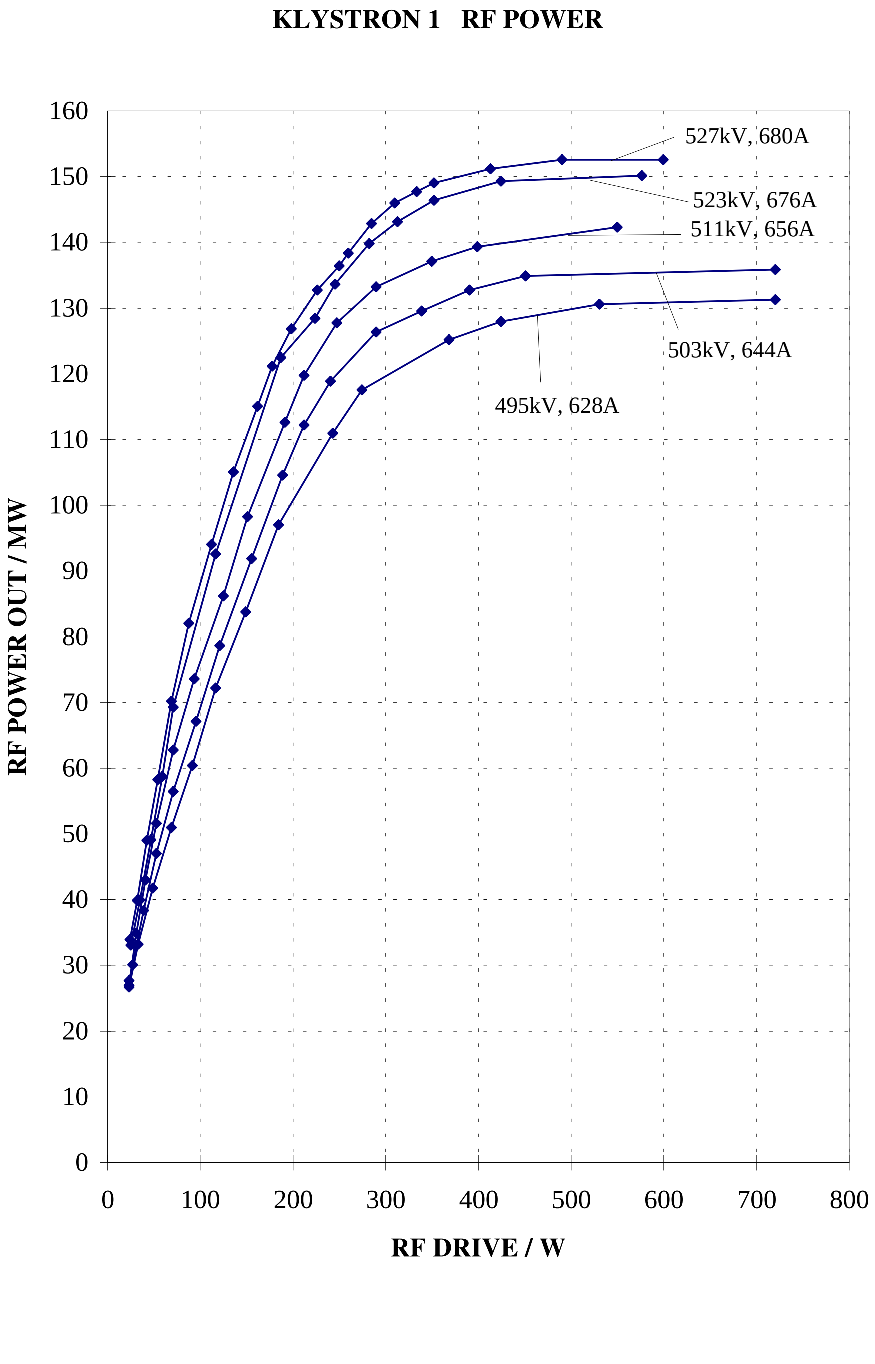

Figure 4.2.24: *RF power versus drive power for test facility klystron 1*

failures although the power per window is increased. In this case the window in one waveguide has to transmit 75 MW instead of 37.5 MW. Further research on window materials must be performed to achieve this goal. Besides these considerations, the output waveguide assembly represents an expensive part of the klystron, which makes the entire production process costly. Another possibility to reduce the costs for a klystron is the gun assembly. A gun for instance without a big tapered ceramics would make the fabrication of a klystron easier and cheaper, too.

The maximum efficiency achieved with the klystrons for the test facility was 45 % which is almost sufficient for the linear collider. It is a well known fact that if the perveance of a klystron decreases the efficiency increases (for instance see [34]). This means that the beam voltage needs to be increased and the beam current must be decreased. On the other hand one has to take into account that the the beam voltage must be still controllable and can not exceed technologically feasible limits. The proposed solution is a klystron operating at a micro-perveance of 1.0×10^{-6} A/V$^{3/2}$. An efficiency of 55 % could be achieved and the beam voltage is kept at 595 kV, which is only about 10% above the voltage of the test facility klystrons. Decreasing the micro-perveance from 1.8 to 1.0×10^{-6} A/V$^{3/2}$ in addition supports the construction of a klystron using periodic permanent magnet focusing (PPM). Because the beam current decreases, the effect of the space charge forces in the beam is reduced and the beam confinement is easier. Table 4.2.5 presents the design parameters of a 150 MW S-Band klystron with micro-perveance 1.0×10^{-6} A/V$^{3/2}$.

Peak Power Out	150 MW
Pulse Duration	2.8 μs
Repetition Rate	50 Hz
Average Power	21 kW
Beam Voltage	595 kV
Beam Current	459 A
Perveance	1.0×10^{-6} A/V$^{3/2}$
Efficiency	55 %
Gain	55 dB
Focusing	Periodic Permanent Magnet (PPM)

Table 4.2.5: *Parameters for a PPM focused S-Band klystron*

At SLAC a PPM focused X-Band (11.424 GHz) klystron with an output power of more than 50 MW and with an efficiency up to 60 % [35] has already been developed. Because of the larger drift tube, the conditions for beam focusing are more relaxed for an S-Band klystron and the development of an S-Band PPM focused klystron should be straight forward. S-Band klystrons operating at an output power of 150 MW are available and their performance has been demonstrated successfully. Some changes, most of them only moderate, are required to achieve the goals demanded for a linear collider klystron.

In parallel to the R & D program discussed before, Thomson [5] has developed a 150 MW klystron as well and the results have recently been presented [33]. This, as a matter of fact, proves the industrial available capabilities, specifically at S-Band. This klystron requires a higher beam voltage (up to 590 kV) as compared to the test facility klystrons, but less current. The micro-perveance is $1.35\times10^{-6}\,\mathrm{A/V}^{3/2}$. About 2 kW of drive power are necessary to saturate the klystron. Up to now this tube has been tested at 1 μs pulse duration and a repetition rate of about 1 Hz.

Other companies with well known capabilities in this field have as well offered, as a first step, to rebuild the 150 MW tube which resulted from the common R & D program at SLAC. This represents, to our opinion, a strong basis of future R & D for the development of a PPM focused S-Band tube.
Industry type production lines have been investigated for this klystron [36] and show cost reductions which reach the final per item cost goal taking into account the anticipated production number per year, both for first installation and for the continuous exchange and upgrade in the linear collider as well. In this study a dedicated klystron facility is proposed with a plant being designed to finally produce approximately 1000 klystrons per year with an increasing yield starting from 40 % and over the first four years going up to 100 %.

Apart from the production of the klystron, the mean time to repair (MTTR) is a major issue for the operation of a linear collider. As already mentioned, even with the anticipated lifetime of 50,000 hours every 20 hours a klystron has to be changed, while the accelerator is operating. Assuming 5,000 hours of operation 250 klystrons per year have to be transported into the tunnel, and brought back to the klystron factory for repair. Clearly the capability for klystron replacement must be higher than the rate for klystron failure. A semi-automatic exchange and start up procedure in the collider tunnel is conceivable. It should allow a klystron replacement and start up with a minimum of activies, which must be performed by specially skilled personal. These considerations must be already taken into account for the klystron design and its mechanical layout. Collaborations with automatization specialists and klystron manufactures should be settled. A first investigation of the replacement process has already been performed [37].

4.2.6.2 Line Type Modulator

Line type modulators represent the type of modulator which is most used for the production of high power, high voltage pulses. Almost all pulse klystrons at linear accelerators in the world make use of line type modulators, for instance all 240 klystrons at the SLC at SLAC are supplied by line type modulators [38]. Line type modulators therefore represent a well established and proven technique and therefore are one possible choice for the generation of pulse power at the S-Band linear collider. The following pages represent the status of the development of line type modulators for the 150MW S-Band klystrons. After presenting the status, parameters of a line type modulator

[5]Trademark of the French company THOMSON CSF

meeting the demands of an S-Band linear colldider will be given and a possible setup will be shown.

The present status of line type modulators for the 150 MW klystrons is given by the modulators for the S-Band test facility [39]. The facility requires two line type modulators for the generation of high voltage pulses for two 150 MW klystrons. The requirements for these modulators are determined by the klystron parameters (see klystron chapter), i. e. by the cathode voltage and current, the pulse duration and repetition rate. The numbers for the line type modulators are listed in Table 4.2.6, the circuit is shown in Fig. 4.2.25.

Pulse Voltage	535 kV
Pulse Current	700 A
Flat Top Pulse Duration	3 μs
Repetition Rate	50 Hz
Equivalent Square Wave Duration	4.8 μs
Rise Time 10 - 90%	700 ns
PFN	four lines parallel, each line ten sections
PFN impedance	1.34 Ω
Total Capacitance	1.8 μF
Capacitor Capacitance C_i	45 nF
Coil Inductance L_i	1.3 μH
Charging Voltage	50 kV max.
Peak Current (primary side)	16 kA
Pulse Transformer Ratio	1 : 23

Table 4.2.6: *Parameters of the present line type modulator for the S-Band test facility.*

The PFN is charged by resonant charging up to twice the power supply voltage. The total PFN capacitance of 1.8 μF together with the charging choke inductance of 16 H gives a charging time of 17ms. The HV power supply is rated to a maximum voltage of 26.5 kV and an average current of 5A. Because the HV power supply is SCR controlled, which leads to a pulse to pulse voltage stability better than 1%, it is not necessary to use a de-Qing system. The PFN consists of four lines in parallel with ten PFN sections per line. The nominal PFN impedance calculated by $Z=1/4(L_i/C_i)^{1/2}$ is 1.35 Ω. Two lines of the PFN are connected to one thyratron. This reduces the maximum pulse current per thyratron to less than 10 kA. The two thyratrons can be triggered independently by two thyratron drivers. The PFN energy is transferred by a 1:23 step up transformer into the klystron. The klystron impedance at the nominal secondary pulse voltage of 535 kV and 700 A is 764 Ω, which represents an impedance of 1.44Ω to the PFN, i.e. there is a slight positive mismatch. The rise time of the high voltage pulse of 700 ns is mainly determined by the pulse transformer with the

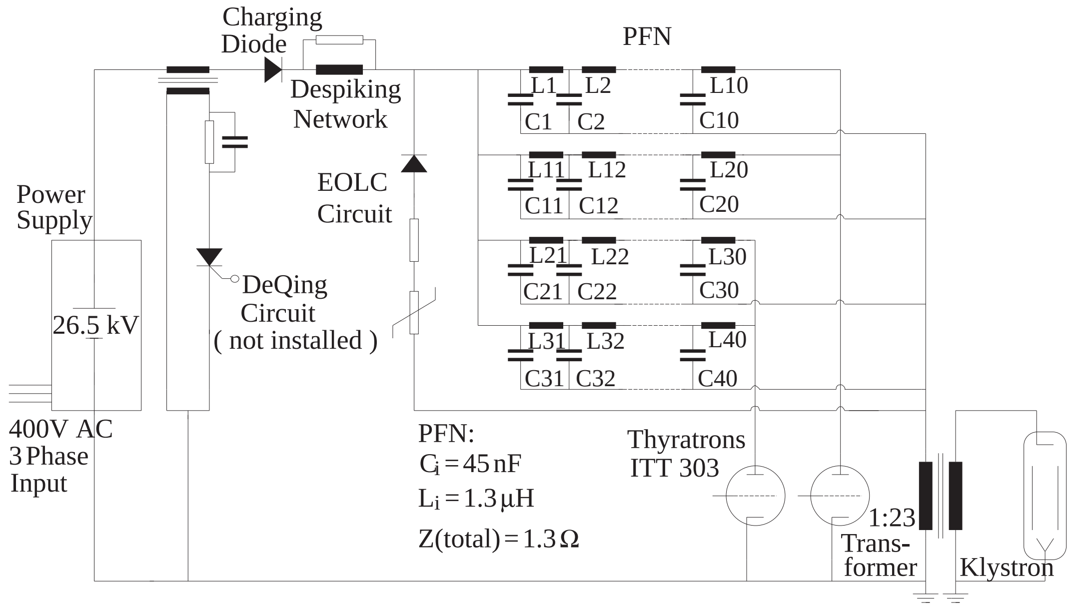

Figure 4.2.25: *Schematic drawing of the circuit of the present line type modulator at the S-Band test facility.*

transformer ratio of 1:23 and the finite number of 10 sections per PFN line. An end of line clipper circuit (EOLC) made by resistors, varistors and a diode absorbs the energy stored in the PFN in case of klystron arcing. Typical waveforms are shown in Fig. 4.2.26.

The modulator consists of five separate units in total, the PFN unit with the pulse transformer tank, the charging unit, the HV power supply, a control unit and the power supplies for the klystron solenoid.

The PFN unit is 2.6 m high and requires a ground space of 1.5m times 1.4 m. The PFN with its capacitors and coils, the EOLC, the thyratrons and their drivers are installed in this unit. The PFN capacitors are mounted horizontally with one side connected to the aluminum mounting rack. The coils are connected to the other side. The inductances of the coils can be adjusted by c hanging the tap on the coils and changing the position of a slug inside the coil. This allows to tune the shape, especially the flat top of the HV voltage pulse.

The pulse transformer tank is directly connected to the PFN unit. The oil filled tank has a diameter of 1.2 m and a height of 1.6 m. Besides a filament transformer, a blocking coil and some diagnostics like a capacitive voltage divider and current monitors, the pulse transformer is the biggest component in the tank. The connection between the transformer and the PFN unit is made with a transmission line like feed through. It consists of three parallel copper bands, one band is connected to the PFN capacitor mounting rack, the other two are connected to the thyratrons. The klystron with the solenoid sits on top of the tank with the cathode and gun ceramics in the tank oil.

The charging choke and diode and the despiking network are installed in the charg-

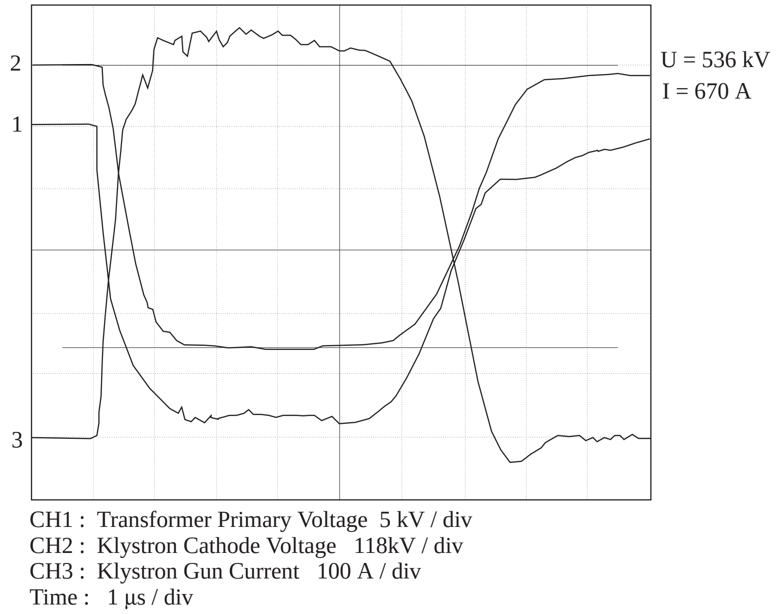

Figure 4.2.26: *Typical waveforms of the line type modulator at the S-Band test faciltiy (without efforts to tune the PFN)*

ing unit. It has a height of 2.45 m and is 1.45 m times 1.35 m wide.

The HV power supply is a commercial power supply. It is 2.25 m high and 1.4 m times 1.85 m wide. It can be operated locally or remotely via a GPIB interface.

All controls are installed in four nineteen inch racks. It is possible to control the modulator locally and remotely by these racks. About two racks are occupied by scopes and printers, which were required during commissioning. The interlocks are accomplished by a programmable logic controller, which also serves for data logging of analog signals like cooling flow rates, temperatures and vacuum pressures. The vacuum power supplies for the klystron, heater power supplies for klystron and thyratrons, bucking coil power supply and trigger generators are also installed in the control rack. The solenoid power supplies require the space of three nineteen inch racks.

The total efficiency of the modulator at the test facility reaches 58%. It is defined by the power transferred to the klystron during the 3 μsec flat top of the HV pulse, devided by the wall plug power. The efficiency contributions of the HV power supply and the resonant charging system are each nearly 94%. This means that most of the wall plug power, which can not be used for RF generation, is lost during the energy transfer from the PFN to the klystron. Only the flat top of the HV pulse can be used for RF generation. Besides a small fraction of ohmic losses during the HV pulse, it is mainly the energy during the rise and fall time of the HV pulse, which is lost.

Power required for the auxiliaries like the filaments, drivers, core bias or solenoid power supplies has not been taken into account for the numbers above. A comparison of the total power required per modulator and the power for the auxillaries for the test facility modulator and the modulator foreseen for the Linear Collider is given in table 4.2.8

Adding these numbers together a wall plug power of 87 kW is required for one line type modulator at full repetition rate and output power, plus about 20 kW for the solenoid and auxiliaries, which is clearly not acceptable for a large scale installation. The goal for the modulator efficiency from wall plug to klystron without auxiliaries is 70%.

In order to enhance the efficiency of the present modulator and to meet the demands of a future PPM focused klystron, further development of the existing line type modultors is required. Therefore it is necessary to have a closer look at the reasons for the losses in the present modulator.

The dominant loss in the present modulator is due to the limited power transfer from the PFN to the klystron. As explained above, this is mainly due to the power lost during the rise and fall times of the HV pulse. Two effects determine the rise and fall times of a modulator, the number of sections per PFN line and the characteristics of the pulse transformer. As a rule of thumb the rise time T_r of a PFN consisting of N sections is given by $T_r=T/N$, where T is the equivalent square wave duration. For the modulators at the test facility for instance where T is 4.8 μs and N is 10, one calculates 480 ns. Another important effect on the rise time is caused by the characteristics of the pulse transformer. Two parameters of a transformer limit the rise time. The first is the leakage inductance of the transformer. The coupling between the primary and secondary side of a pulse transformer can never be ideal due to the necessary insulation between the primary and the secondary high voltage side. A part of the magnetic field produced by the primary side does not pass through the secondary winding of the transformer, which leads to a leakage inductance in series with the load. The second parameter is the capacitance between the primary and secondary winding. This capacitance, the stray capacitance of the klystron cathode and the transformer to ground in addition must be charged during the HV pulse.The higher these capacitances are the longer is the rise time. Experience shows that decreasing the step up ratio of a transformer decreases the leakage inductance and the capacitance between primary and secondary winding, which leads to faster rise and fall times.

A trade off must be made between these considerations and the fact that decreasing the step up ratio of the pulse transformer leads to an increase of voltage on the primary side, i.e. an increase of charging voltage of the PFN. The availability of HV power supplies, low inductance capacitors and thyratrons must be taken into account. Assuming that 75 kV is a technically feasible limit for the voltage on the the PFN and that a future klystron operates at 595 kV, a step up ratio of 1:16 for the transformer ia applicable. By using 1:17 instead, a charging voltage of 70 kV is required. This leaves some safety margin if more voltage would be required. The parameters for a future modulator are shown in Table 4.2.7. A shorter flat top pulse duration of only 2.8 μs is required by the klystron. Figure 4.2.27 shows the schematic of the circuit.

The PFN has two lines in parallel. Each line consists of 20 sections. The contribution of the PFN rise time to the total rise time calculated by the rule of thumb formula given above is less than 200ns. The decrease in step up ratio also lowers the pulse cur-

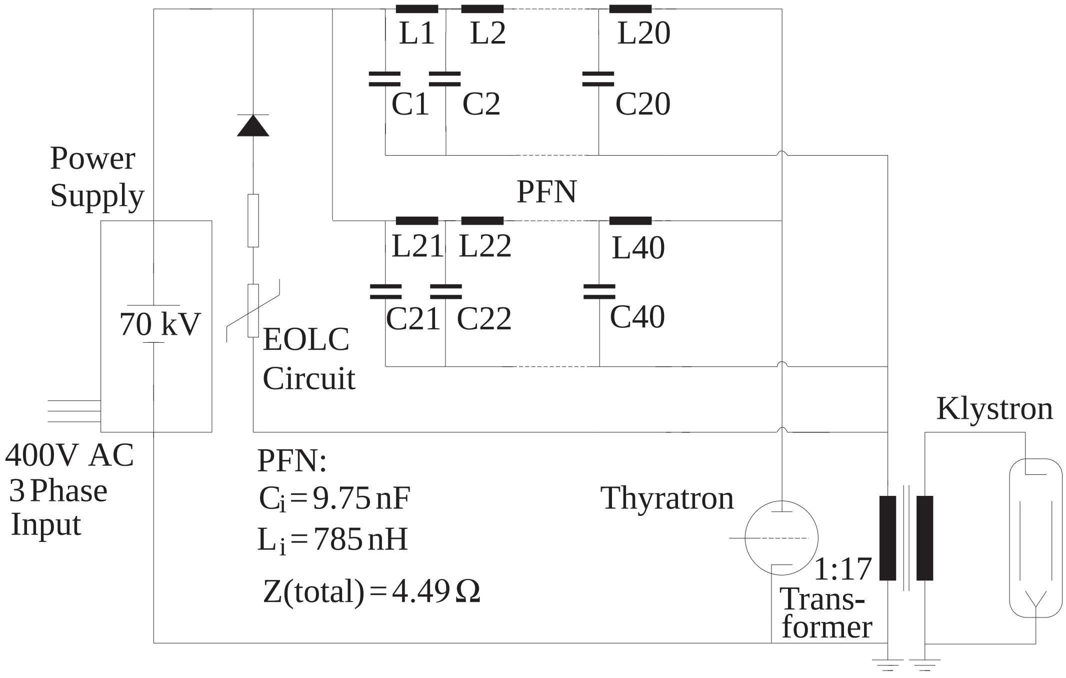

Figure 4.2.27: *Schematic drawing of the circuit of a future line type modulator*

rent on the primary side to 7.8 kA. Thyratrons capable of more than 70 kV and 10 kA are already available from industry. This allows to reduce the number of thyratrons per modulator from two to one, thus reducing the investment and the operations costs .

With the numbers in Table 4.2.7 one obtains an efficiency of 80% for the power transfer from the PFN to the klystron. Taking into account ohmic losses by introducing a factor of 0.97 one gets an efficiency of 77% from the PFN to the klystron. Power is also lost during the resonant charging process of the PFN. This is mainly due to ohmic losses in the huge charging choke, which has a resistance of about 100 Ω, and other components in the charging path. Installing a DeQing system would further decrease the efficiency.

Fortunately inverter power supplies are available today, which allow a direct charging of a PFN to the desired voltage with a good regulation (for instance from Maxwell, San Diego, USA). Resonant charging and DeQing is no longer necessary. The supplies available at the moment are limited to 50 kV, but this is mainly because of the limited demands for higher voltage up to now. An extensions of this technique to higher voltage should be possible with only small effort. By using these supplies, almost no losses would appear between power supply and PFN during the charging process. The intrinsic efficiency of these supplies from wall plug to power supply output is 92%. Therefore it can be assumed that an efficiency of 92% from wall plug to the PFN can be reached.

Inverter power supplies require a protection against voltage reversal, which is usually achieved by installing a protecting diode at the output of the supply. Since an

Pulse Voltage	595 kV
Pulse Current	459 A
Flat Top Pulse Duration	2.8 μs
Repetition Rate	50 Hz
Equivalent Square Wave Duration	3.5 μs
Average Output Power	47.8 kW
Rise Time 10 - 90%	500 ns
PFN	two lines parallel, each line twenty sections
PFN impedance	4.49 Ω
Total Capacitance	390 nF
Capacitor Capacitance C_i	9.75 nF
Coil Inductance L_i	780 nH
Charging Voltage	70 kV
Peak Current (primary side)	7.8 kA
Pulse Transformer Ratio	1 : 17

Table 4.2.7: *Parameters of a future line type modulator*

EOLC diode must be installed at the PFN on the HV power supply side for klystron protection reasons anyway, a careful design of this circuit will protect the power supply, too, and no additional components would be required. Inverter power supplies can be built in a modular way. Many modules in parallel represent one supply. By installing one spare module per supply one can run the power supply even in the case that one module fails. The input voltage of the supplies usually is 400 V, three phase, 50 Hz, but it is conceivable to allow an input voltage up to 1000 V, which would further reduce the transfer losses in the tunnel.

Multiplying the number for the power supply efficiency of 92% with the number for the pulse efficiency of 77% one gets a total modulator efficiency of 71% from wall plug to the klystron. Assuming the klystron efficiency of 55%, the power demand from wall plug per modulator is 54 kW.

As for the modulators at the test facility the power for the auxiliaries is not included in this number. The power required by the auxiliaries is given in Table 4.2.8. The power for a solenoid is not included, because it is assumed that a klystron for a linear collider would be PPM focused.

The modulator would basically consist of three main components, the PFN unit with the pulse transformer tank, the HV power supply and a local control unit.

The size of the PFN unit would be approximately the same as for the modulators for the test facility. The mounting of the different components in the cabinet could be done in almost the same way as for the modulator at test facilty. The PFN unit at the test facility was built with a safety margin for the distances of the high voltage components, which allows to increase the voltage. The same holds for the pulse transformer tank. In any case, both components must be transportable in the tunnel via the installed transport system.

	SBTF	**LC**
rf pulse length	3.0 μsec	2.8 μsec
Klystron efficiency	45 %	55 %
electric efficiency AC to HV flat top	58 %	77 %
power required for HV production	86 kW	54 kW
Klystron filament	1.3 kW	1.3 kW
Thyratron filament and reservoir	1 kW	0.5 kW
Core bias power supply	0.3 kW	0.3 kW
Solenoid	15 kW	–
Other	2 kW	2 kW
Total	19.6 kW	4.1 kW

Table 4.2.8: *Power demands for the high voltage supply of the klystron as well as the auxiliaries of the line type modulator at the S-Band test facility and the modulator foreseen for the Linear Collider. The number listed under SBTF (S-Band Test Facility) have been achieved up to date.*

The power supply fits in one nineteen inch rack of 2.5 m height. It is also conceivable that one uses two of the racks with reduced height if more space is required. Existing supplies operating at the same power level confirm these assumptions.

The control unit has to take the auxiliary supplies and the programmable logic controller for the interlock. Two nineteen inch racks are required for the installation.

A possible setup of a future line type modulator is shown in Fig. 4.2.28.

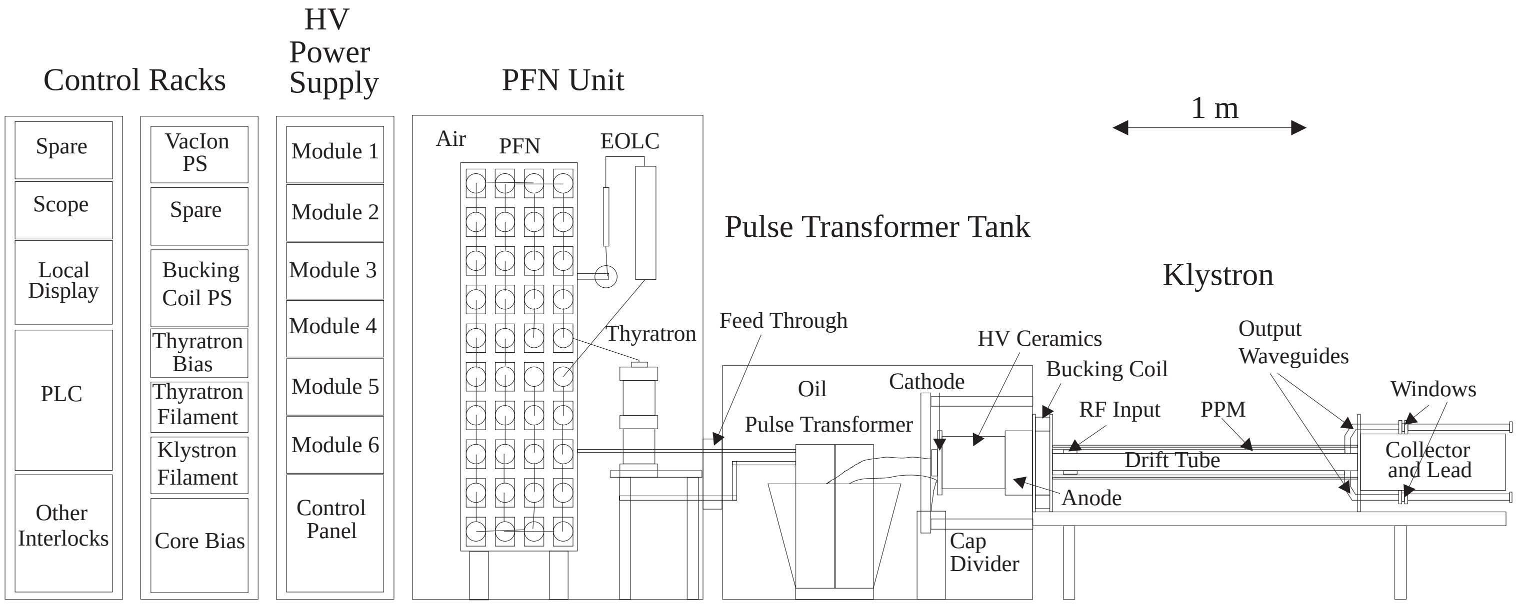

Figure 4.2.28: *Possible setup of a future line type modulator*

4.2.7 Rf Drive System

Description of the Problem In a linear collider, the drive line is the power feed line which is used to excite the high power klystrons, along the linac tunnel. In the proposed 500 GeV center of mass S-Band linear collider, 2500 klystrons will require approximately 400 W drive power each. These klystrons are distributed along the 30 km long accelerator. Therefore approximately every 12 m the drive line has to deliver this amount of power with the appropriate phase and amplitude control within one pulse and with the required pulse to pulse stability.

So far different ideas have been discussed to solve this problem. For example, a low power glass fiber could be used to drive a solid state preamplifer in front of every klystron, or a special drive klystron could power groups of klystrons. While the first version turns out to be a rather cost intensive one, it has certainly the greatest flexibility, because the low power rf can be manipulated in front of every klystron. The second version is certainly cheaper but also requires a widely distributed rf control network. Both systems involve a dedicated distribution system for the low power rf and consist of a large number of components which tend to fail or have to be replaced according to the lifetime.

Therefore a technical solution will be discussed which is based on the idea of using a single high power drive line for many klystrons. This drive line would be powered by the same type of klystron used to feed the accelerating structures (150 MW peak power) and is a passive system which should not require any maintenance. Such a drive line system has a number of drawbacks but also many advantages.

The main problem of a very long drive line is dispersion and energy propagation velocity. The rf pulse which fills the accelerating structure and accelerates the beam is only $2.8\,\mu$s ($\approx 900\,$m) long. To excite every klystron in time, the drive pulse has to travel with the speed of the beam pulse, here the velocity of light, along the linac. At the same time the pulse shape (amplitude and phase) is not allowed to change (mainly due to dispersion and mode conversion), especially if phase or amplitude modulation is used within each single rf pulse.

Ridge waveguide as a drive line A drive line concept based on a ridge waveguide [40], see Fig. 4.2.29, has been developed which allows a large number of the high power klystrons to be fed with a single drive line. This type of waveguide fulfills requirements which are necessary for a drive line, namely, low losses, low signal distortion due to dispersion and good suppression of higher order modes. With this concept it should be possible to cover at least a length of 3 km with a single drive line if one of the high power klystrons is used to generate the drive signal.

Dispersion In a waveguide which does not support a TEM mode, signal distortion occurs due to the non-linear frequency dependence of the propagation constant β. Different portions of the signal travel with different velocities so that the output signal becomes dispersed. Nevertheless, for narrow band signals β may be approximated by a linear function throughout the frequency band of interest. In this case the transmitted

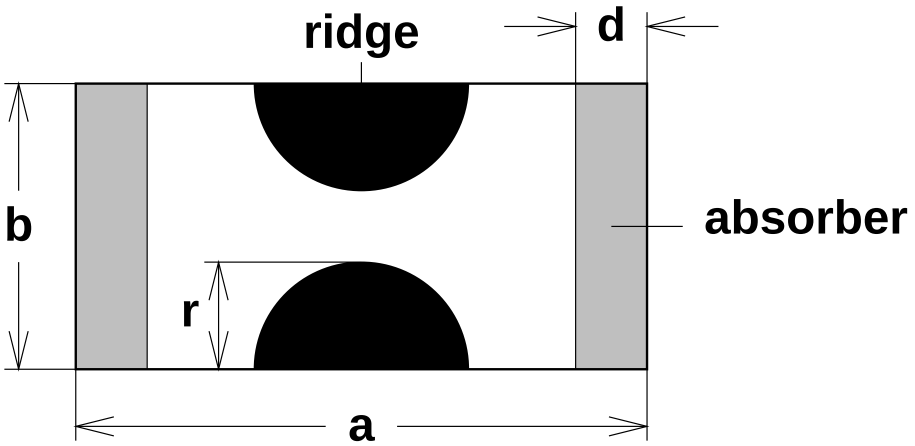

Figure 4.2.29: Cross section of a ridge waveguide with circular ridges and absorbers at the side walls.

signal is identical to the input signal, apart from the amplitude and a time delay. Let us assume a bandwidth of 1 MHz and a group velocity of $v_{gr} = 98\% \cdot c_0$. With these parameters and a length of the drive line of 3 km, one obtains a transmission time error of about 0.15 ns which is small compared to the rf pulse length. From this point of view an even larger dispersion (lower group velocity) would be permissible.

Nevertheless one has to keep in mind that, if the group velocity is smaller than the velocity of light, delay lines with well-defined length have to be inserted between the drive line and each individual klystron feed, in order to keep the drive pulse synchronous to the particles. In our case, the length of the first delay line is 60 m whereas the last klystron feed is directly connected to the drive line. In between, the length of the delay lines has to be linearly decreased. For practical reasons one would realize the delay lines as coaxial cables which unfortunately suffer from a high damping, typically 0.4 dB/m. Hence the first delay line leads to an additional damping of 24 dB which is not serious because the full klystron power of 150 MW is available at the beginning of the drive line.

Suppression of higher order modes In order to keep the signal delay and dispersion small it cannot be avoided to use a highly overmoded waveguide. Two serious effects arise from the excitation of higher order modes. Obviously some of the power in the fundamental mode is lost if it is converted into other modes with higher damping. The second more serious effect gives rise to signal distortion if the fundamental mode is converted into higher order modes and some of the power of these modes is converted back into the fundamental mode at a position farther along the waveguide. In order to avoid signal distortion by conversion and re-conversion the undesired modes have to be suppressed (attenuated) to avoid re-conversion.

Nevertheless such an overmoded waveguide may be used if one can control the higher order modes. In a ridge waveguide, the electro-magnetic field of the fundamental mode is concentrated in the vicinity of the ridges whereas higher order modes extend

Mode	Case 1	Case 2	Case 3	Case 4
α_f in dB/km	7.11	3.29	8.04	9.66
α_{h1} in dB/km	6.71	$3.93\cdot10^3$	$1.94\cdot10^1$	$4.15\cdot10^1$
α_{h2} in dB/km	6.85	$3.95\cdot10^3$	$1.96\cdot10^1$	$4.18\cdot10^1$
α_{h3} in dB/km	6.14	$3.51\cdot10^1$	$1.29\cdot10^1$	$2.50\cdot10^1$
α_{h4} in dB/km	9.93	$8.28\cdot10^1$	$2.52\cdot10^1$	$5.20\cdot10^1$
α_{h5} in dB/km	$1.18\cdot10^1$	$1.91\cdot10^3$	$2.81\cdot10^1$	$5.67\cdot10^1$
α_{h6} in dB/km	$1.12\cdot10^1$	$1.94\cdot10^3$	$2.80\cdot10^1$	$5.74\cdot10^1$
α_{h7} in dB/km	$3.00\cdot10^1$	$4.12\cdot10^3$	$8.15\cdot10^1$	$1.71\cdot10^2$
α_{h8} in dB/km	$3.09\cdot10^1$	$4.20\cdot10^3$	$8.42\cdot10^1$	$1.77\cdot10^2$
α_{h9} in dB/km	$2.53\cdot10^1$	$7.01\cdot10^2$	$6.07\cdot10^1$	$1.23\cdot10^2$

Table 4.2.9: Attenuation constants α_f and $\alpha_{h1}\ldots\alpha_{h9}$ for the fundamental mode and the propagating higher order modes, respectively, of a ridge waveguide.
Case 1: Empty drive line made of copper (Conductivity= $5.8\cdot10^7$ S/m).
Case 2: Additional damping due to absorbers at the side walls.
Case 3: Steel shielding (Conductivity = $0.5\cdot10^7$S/m).
Case 4: Kanthal shielding (Conductivity = $0.1\cdot10^7$S/m).

throughout the cross section of the waveguide. Hence these modes can be suppressed by suitable absorbers located at the side walls. A similar effect can also be achieved by lossy side walls made of steel or Kanthal.

Numerical results A ridge waveguide with shielding dimensions of $(a = 200\,\text{mm}) \times (b = 100\,\text{mm})$ and a ridge radius of $r = 33\,\text{mm}$ is assumed. Due to the high field strength in a drive line it is not recommended to use rectangular ridges which may lead to discharge at the sharp edges. Instead of this, circular ridges seem to be most suitable. Figs. 4.2.30–4.2.33 show the transverse field distributions of the four propagating modes with the lowest cutoff frequencies which have been computed with the MAFIA program package [4]. Keeping in mind that the density of the field lines is proportional to the field strength, Fig. 4.2.30 demonstrates that the fundamental mode is well concentrated at the ridges. The group velocity of this mode amounts to $98.4\% \cdot c_0$ which means that for a 3 km long drive line a coaxial delay line of 48 m, see Fig. 4.2.34, has to be used at the first klystron feed (corresponding to an insertion loss of 19.2 dB).

In Table 4.2.9 the attenuation of the fundamental and the propagating higher order modes is presented for various cases. Case 1 means that we consider an empty drive line completely made of copper. The attenuation of the dominant mode amounts to 7.11 dB/km which corresponds to a damping of 21.3 dB for a 3 km long drive line. Note that in the empty ridge waveguide the attenuation of the some higher order modes is approximately the same or even less than that of the fundamental mode. The situation changes completely if we insert a lossy material at the side walls of the shielding. Two

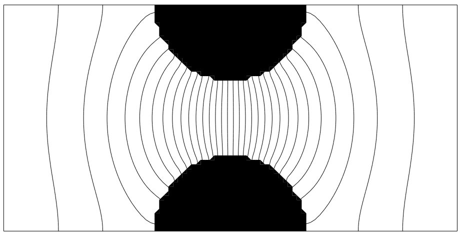

Figure 4.2.30: First TE mode.

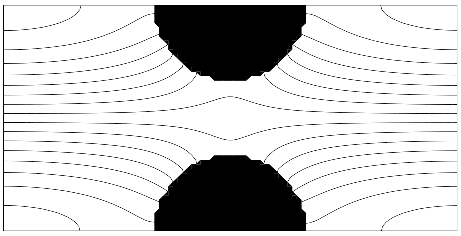

Figure 4.2.31: Second TE mode.

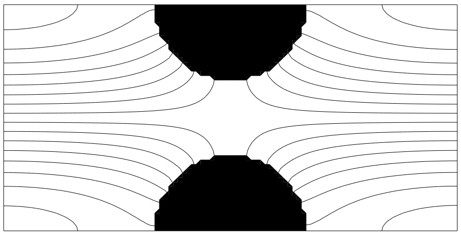

Figure 4.2.32: Third TE mode.

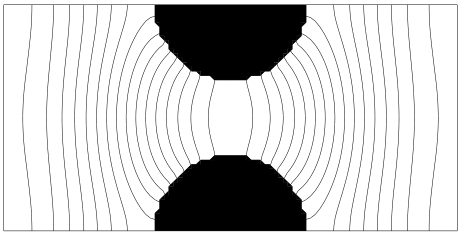

Figure 4.2.33: Fourth TE mode.

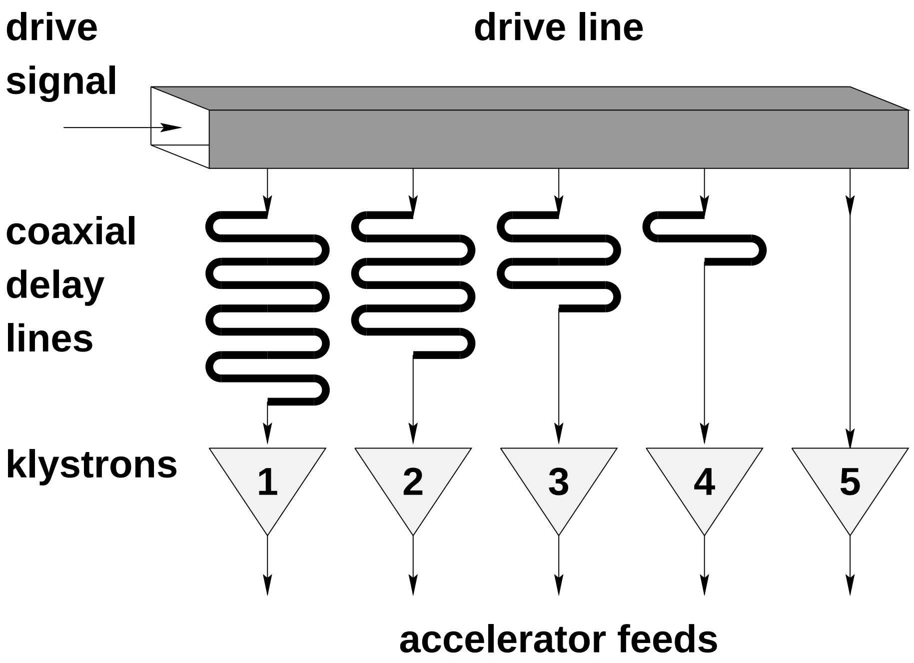

Figure 4.2.34: Schematic drawing of a drive line system with five feeds in which the group velocity of the drive line is less than the velocity of light.

absorbers with a thickness of $d = 4\,\mathrm{mm}$ and a loss tangent of 0.2 are assumed (case 2). Table 4.2.9 gives the additional damping due to the absorbers. The attenuation of the fundamental mode is increased by only 3.29 dB/km whereas the absorbers give rise to a damping of the higher order modes of at least 35.1 dB/km (third higher order mode) which seems to be strong enough in order to guarantee mode stability.

Since it may be difficult to find absorbers which simultaneously satisfy the high power and the vacuum requirements, it has also been investigated whether a sufficient suppression of higher order modes can be achieved by a lossy shielding, i.e., a shielding made of steel or Kanthal. Results for a ridge waveguide with a steel shielding are also given in Table 4.2.9 (case 3). The ridge is still assumed to be made of copper. The numbers presented in Table 4.2.9 demonstrate that the steel shielding has only a minor influence on the damping of the fundamental mode whereas the attenuation of the higher order modes is significantly increased. Nevertheless the mode selectivity is not nearly as good as with the absorbers. In order to get a sufficient damping of the higher order modes the conductivity of the shielding has to be further decreased. With a conductivity of $0.1 \cdot 10^7\mathrm{S/m}$ an acceptable suppression of the higher order modes can be obtained (case 4).

In any case, the overall damping of a 3 km long drive line amounts to approximately 30 dB. In order to keep the mode conversion small at the klystron feeds, the coupling at each individual feed should not exceed $-20\,\mathrm{dB}$ leading to an total attenuation of about 50 dB which is tolerable.

4.2.8 SLED Pulse Compressor Option

In our reference design two six meter long accelerating structures are directly powered by one klystron. With this set-up a loaded gradient of 17 MV/m is achieved at a design beam pulse length of $2\,\mu$s. In this section, we discuss the option of using a pulse compression system (SLED) which enhances the rf-peak power at the structures at the expense of shortening the pulse length. The operation of such a system has been calculated elsewhere in detail and proven by measurements at many accelerator laboratories around the world [41]–[45]. In the particular case considered here, one klystron still feeds two six meter long structures. Nevertheless a higher loaded gradient is achieved and thus an energy upgrade of the collider is realised without the need to increase the number of pulsed rf-sources.

The SLED concept uses two additional storage cavities with a high quality factor which are charged over the first part of the klystron pulse. Then the klystron phase is switched by 180deg and the field energy is extracted from the cavity. Fig. 4.2.35 shows the principle behavior of the SLED system with the respective field, cavity charging and accelerating voltage as a function of time. In Fig. 4.2.35, an rf pulse width of $3\,\mu$s is assumed. After $2.2\,\mu$s of operation, the phase switch of the klystron takes place. Taking into account beam loading compensation (see next section), the beam pulse can use approximately 0.5μs of the remaining $0.8\,\mu$s rf-pulse, delivering a beam energy width of approximately 10 percent by compensating the rising part of the accelerating voltage with the negative slope of the beam loading. The higher rf-peak power allows

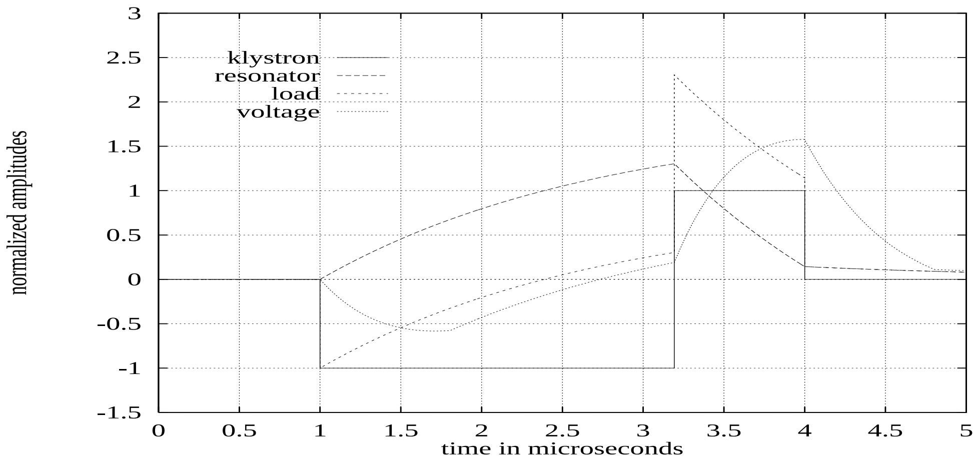

Figure 4.2.35: *Principle operation of the SLED cavity system. All curves show the field amplitudes normalized to the klystron field amplitude which itself is normalized to one. "Load" here means the rf field going to the accelerating structure and "voltage" the integrated acclerating voltage as a function of time.*

SLED cavity parameters		
resonant frequency	GHz	2.998
unloaded Q		180 000
coupling coefficient		13
beam parameters		
number of e^- per bunch		$1.2{\cdot}10^{10}$
bunch to bunch distance	nsec	4
number of bunches		125
performance		
minimum average loaded gradient	MV/m	27.5

Table 4.2.10: *Parameters used for the simulation and gradient achieved with the SLED cavity system.*

to increase the beam pulse current, keeping the fractional beamloading approximately constant. In the simulation we assume a train of 125 bunches with a bunch to bunch distance of 4 ns and a charge of $1.2 \cdot 10^{10}$.

The performance of the proposed SLED cavity system is described in Table 4.2.10 assuming standard parameters for the section and the klystron. The original pulse compressor used at SLAC [41] is based on cavities with $Q_0 = 115000$. In this proposal, cavities with $Q_0 = 180000$ are suggested. In [43], the performance of a cylindrical TE_{038}-cavity with the required properties has already been realized. It turned out that the main problem in the design of such a cavity is, to find an operating mode which is far enough separated from other modes in order to guarantee stable operation.

As shown in Table 4.2.10, a minimum loaded gradient of 27.5 MV/m can be achieved with the proposed SLED system, about a factor of 1.6 higher than for the design without SLED. It should also be taken into account, though, that the overall power transfer efficiency is lower by about a factor of 0.6 compared to the reference design.

4.2.9 Beam Loading Compensation

Description of the Problem For normal conducting linear colliders (compare [46]) the transient beam loading in the accelerating structures is typically of the order of 20-30 %. This results in a multi-bunch energy spread if no cure is foreseen. On the other hand, in a linear collider the transient energy spread has to be controlled down to a few tenths of a percent.

In this section two methods which are suitable for a sufficient compensation of the multi-bunch energy spread are presented, namely, amplitude and phase modulation of the klystron pulse. Both methods can be used with and without SLED system. Since either concept suffers from specific disadvantages, e.g., two drive lines are required for the phase modulation approach, it has not yet been decided which method is to be used. A final decision will be taken based upon measurements on the test facility.

Energy Spread Compensation with the SLED System Let us consider a set-up with SLED system first. In such a scheme the end of the bunch train typically fits the end of the rf pulse. In general, for a given pulse train length which has to be significantly shorter than the decay time of the SLED cavity, there is always a specific current per pulse in order to achieve the same energy at the beginning and the end of the current pulse while in the middle the energy is higher by several percent. For the parameters used here the energy spread remains to be of the order of 10 % for a beam current of $\approx$ 500 mA. Solutions to further reduce the energy spread have been discussed and published already [47, 48]. A typical result is presented in Fig. 4.2.36 using amplitude modulation, where the klystron amplitude is reduced by $\approx$ 30 % and linearly step by step ramped back to the maximum value towards the end of the pulse. In this case, the resulting energy spread is less than 0.2 %.

In a set-up where no SLED cavity is used and the beam pulse is comparable or longer than the filling time of the section, the amplitude ramp would start at the beginning of the rf pulse. A linear amplitude ramp almost perfectly compensates the beam loading of a constant current pulse in a constant gradient section with constant shunt impedance per unit length. This can be seen in Fig. 4.2.38. The rf amplitude (normalized to the maximum amplitude; solid line) and the rf phase (normalized to π; dashed line) are given in the upper graph, while the lower shows the unloaded and loaded accelerating gradient with a beam pulse switched on after one filling time. In the calculation presented in Fig. 4.2.38, the amplitude starts at 23 % of the maximum value. The resulting total energy spread over the bunch train lenght is better than 0.1 % and limited by errors due to the amplitude modulation and klystron power jitter within the pulse. For the case presented in fig. 4.2.36 the resulting energy spread is shown in fig. 4.2.37.

In general, continuous amplitude modulation has the disadvantage of operating the klystron not saturated. This enhances the amplitude and phase jitter which has a negative impact on the performance during the ramp. For a detailed study assumptions on the flatness of the amplitude have to be made and measurements using the test facility are required.

Energy Spread Compensation with two Anti-Phased Klystrons A second method for compensating the transient beam loading will be investigated here. Going off crest in two succeeding klystron stations towards a phase angle (klystron n: $+\phi$ and klystron n+1: -ϕ) will compensate the beam loading at every station and compensates the single bunch energy spread over two stations. Following this strategy, the single bunch energy spread is increased at station n but already compensated at station n+1. The residual effect on the beam emittance from chromatic dilution is estimated to be negligible.

Although it is not foreseen here, even the single bunch energy spread can be compensated using this scheme, as has been described in detail in [49].

Technically the method can be applied by introducing a phase ramp. While the phase of the electric field stored in the section is still at an average phase angle the phase ramp starts travelling through the section over the filling time, comparable to the filling of the section with beam induced field. In Fig. 4.2.39, the rf amplitude (normalized to the maximum amplitude) and the rf phase (normalized to π) are given in the upper graph, while the lower shows the unloaded and loaded accelerating gradient with a beam pulse switched on after one filling time. Here the klystron amplitude is always at the maximum and the klystron operates saturated. Again the resulting energy spread (for bunch nr. 1 and for a bunch after reaching stady state conditions) is shown in figure

Technical Impacts For both methods proposed to compensate the transient beam loading, it is obvious that control for the drive power or the drive phase of the klystrons is required. From the results presented here it is obvious as well, that the drive signal is either the same for all klystrons (compare method 1 used with SLED cavities) or two classes of klystrons (with $\pm\phi_{off}$) with equal drive signals are existing. Therefore one common drive line for one linac (or two drive lines for one linac) could in principle be used and the control problem with the operation and drive for more than thousand klystrons per linac could be reduced by orders of magnitude.

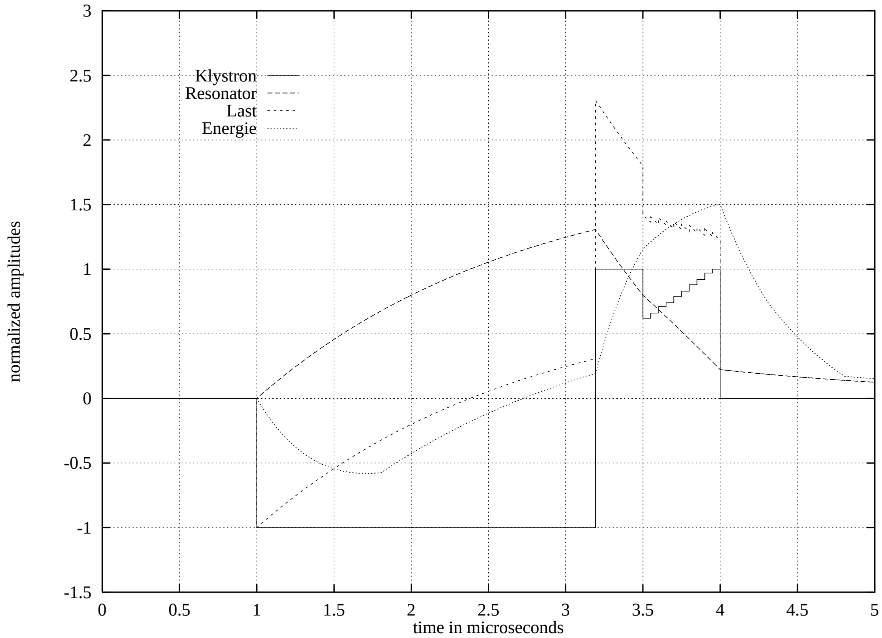

Figure 4.2.36: *Amplitude modulation for optimum compensation of the transient beam loading. The amplitude is reduced after injection and linearly step by step ramped back to the maximum value.*

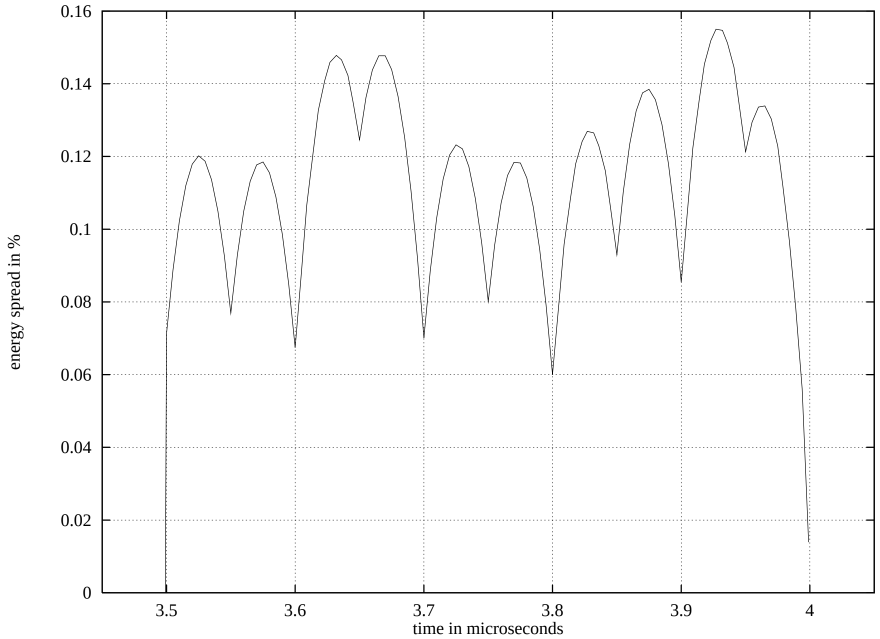

Figure 4.2.37: *The energy spread along the bunch train is shown for the amplitude modulation presented in fig. 4.2.36.*

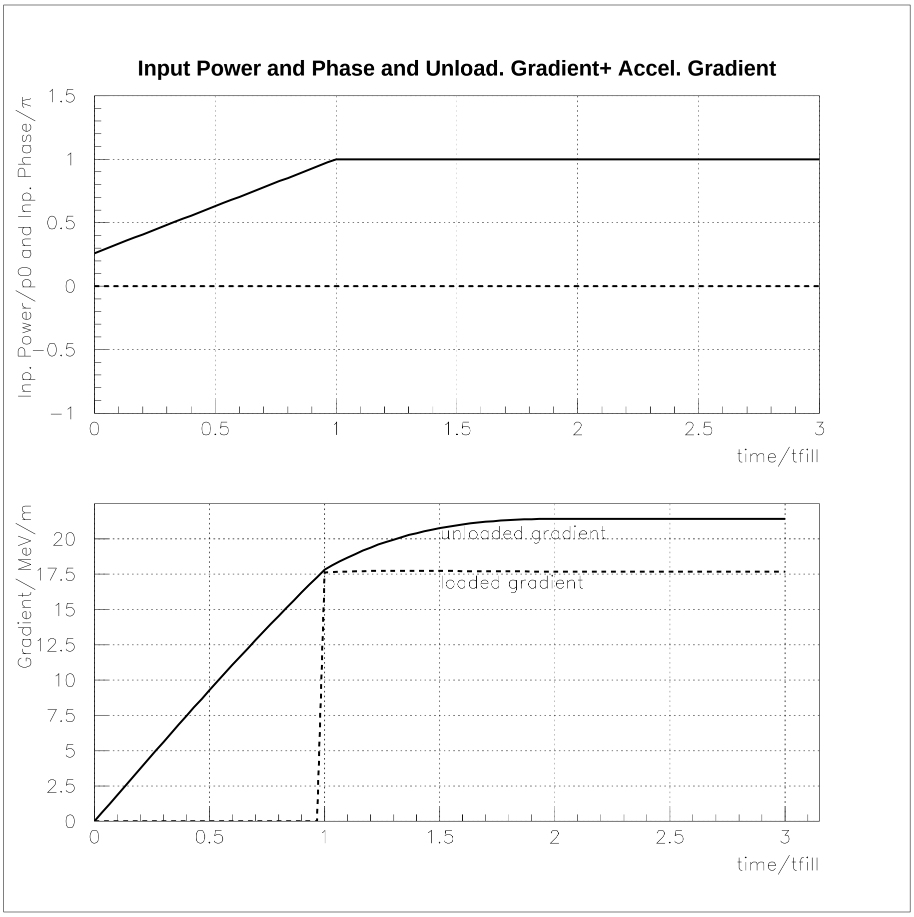

Figure 4.2.38: *Unloaded and loaded gradient with a beam pulse long compared to one filling time and rf amplitude modulation to compensate the beam loading.*

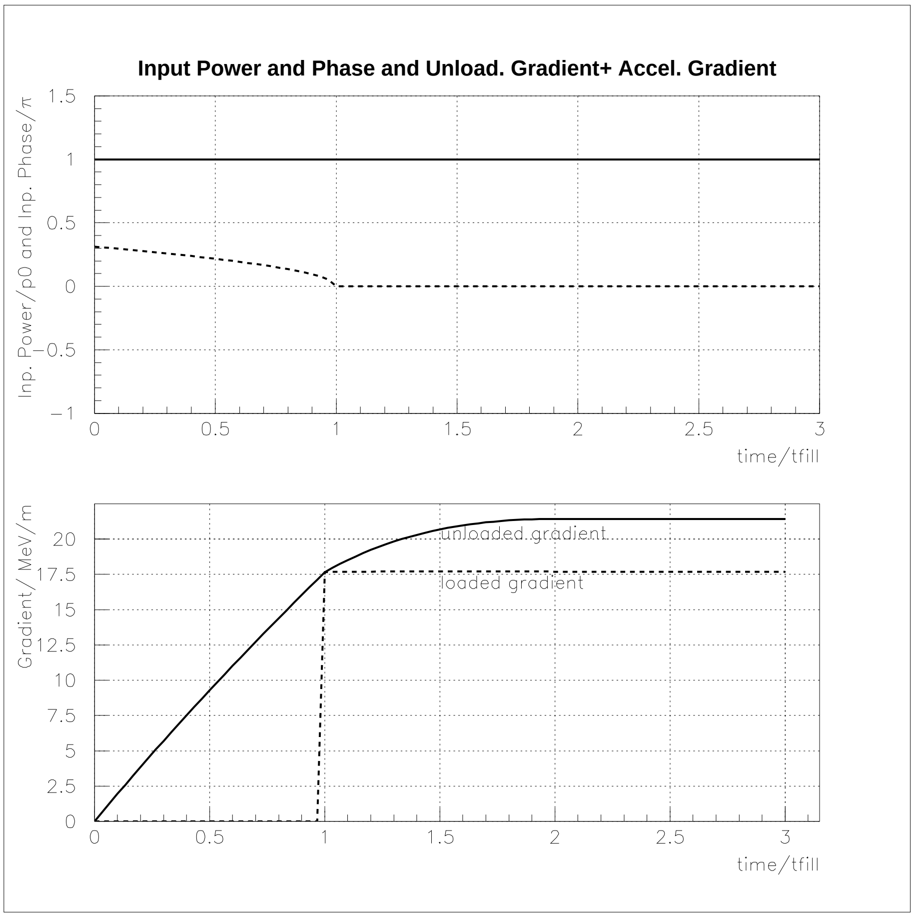

Figure 4.2.39: *Resulting energy spread after phase ramp in front of the accelerating section.*

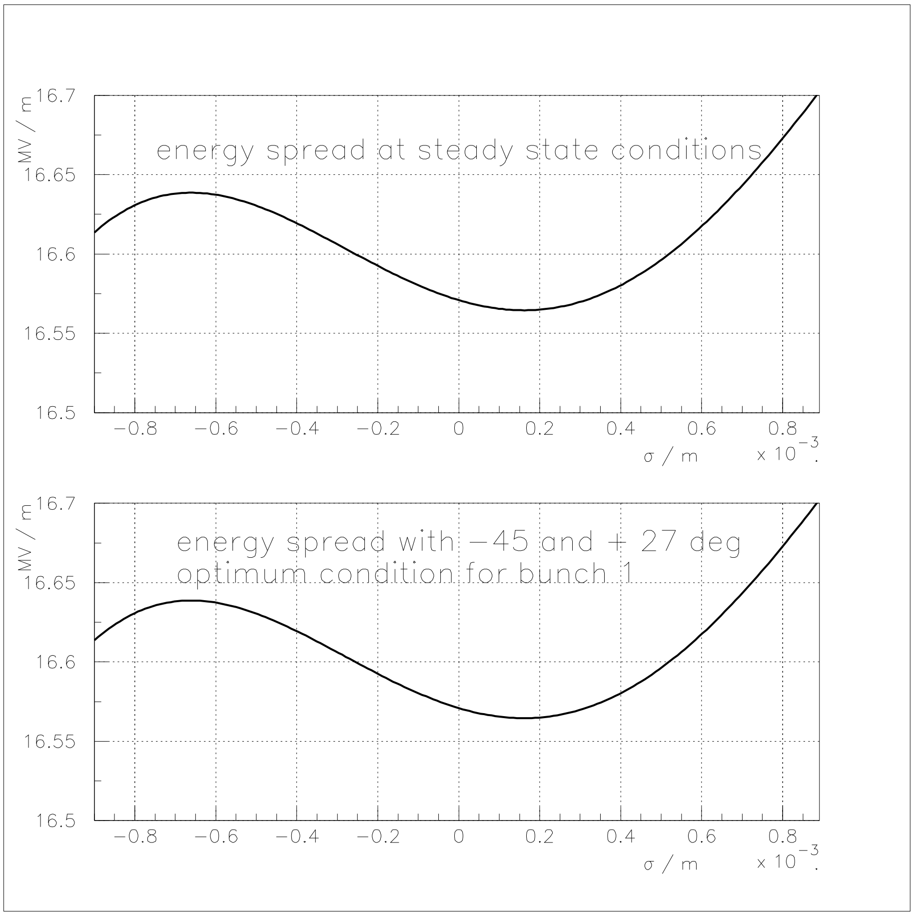

Figure 4.2.40: *The final energy spread for bunch # 1 (start of the rf pulse) and some final bunch after steady state is reached is shown. As can be seen, the single bunch energy width is not disturbed.*

4.2.10 The Quadrupole and Corrector Magnets in the Linac

The linear accelerator will have a FODO structure with 90° phase advance per cell starting from the 3 GeV damping ring towards the end of the linac. While the phase advance per cell is kept constant the FODO cell length changes roughly with the square root of the energy. Overall eight steps are used with a quadrupole magnet between each section in the beginning and having eight accelerating structures in between close to the end of the accelerator. Given a maximum pole tip field of 0.8 T, the length of a quadrupole is given by the high energy end of each of the eight sectors. For optimal beam steering and beam based alignment capabilities, each quadrupole vacuum chamber is equipped with a x/y - strip line beam position monitor, and a **x** as well as a **y** corrector. The correctors are designed with a maximum pole field of 0.1 T which makes air cooling feasible.

The free aperture in the quadrupoles and the correctors is determined by the vacuum chamber diameter. This diameter is constant starting from the cut-off tubes of the accelerating section throughout the quadrupole chamber. This diameter was chosen according to the smallest iris in the section, which allows modes above the cut off frequency of the cut off tube to leave the accelerating structure. These modes travel through the beam pipe and can partly be absorbed at this position or travel into the next strcuture, where the wave will not be in phase with beam any more. The final diameter of the beam pipe is chosen to be 24 mm.

4.2.10.1 The quadrupoles

The quadrupole is a standard magnet with a maximum pole tip field of 0.8 T and an aperture of 24 mm. The necessity to keep the phase advance per FODO cell constant leads to a variation in maximum pole tip fields of not more than a factor of two. Each sector contains one quadrupole type with a given length. The list of quadrupoles and parameters are presented in Table 4.2.11. For the collider and also in the S-Band test facility, quadrupoles are foreseen which have the windings not fixed to the pole but to a separate aluminum support. This support is used to decouple the vibration from water cooling from the pole itself. The concept is described in more detail in 4.8.4.

The total amount of quadrupoles according to Table 4.2.11 is roughly 600 per linac. Every quadrupole will have its own power supply. And the total additional length required for the quadrupoles, the quadrupole chamber and the correctors (one x and one y corrector at every quad) is 600 m over a length of approximately 15 km. Therefore the packing factor is 96% in each of the two linacs. The power consumption per linac will be 1.5 MW for the quadrupoles.

4.2.10.2 The Corrector Magnets

Beside each quadrupole one x and one y corrector magnet is foreseen. The orbit deviation which should be achievable are assumed to be ±5 mm, which is almost the complete aperture of the quadrupoles. The maximum design field is 0.1 T and with approximately 400 windings, the corrector does not need any additional cooling. The

section parameter				
Sector nr	max. Energy	drift space	$L_{m}agn$	nr. of quads tot
	GeV	m	m	
1	12	0.5	0.14	90
2	27	0.5	0.21	75
3	48	0.8	0.28	70
4	75	1.0	0.34	68
5	108	1.0	0.41	66
6	147	1.5	0.47	65
7	192	1.5	0.53	65
8	250	1.7	0.62	73

Table 4.2.11: *Parameters for the Linac quadrupoles in different sectors of the linear accelerator.*

length of the correctors is different in each sector as well and starts from 0.06 m going up to 0.48 m at the end. Because two correctors per quad are foreseen, 2/3 of the required additional length is determined by the corrector magnets. Optimization could slightly reduce this factor at the expense of more electrical power or less kick strength, especially towards the end of the linac, if the x/y corrector winding are on one yoke. So far two separate correctors are foreseen. So far a simple C-type dipole corrector is assumed. In total 1200 corrector magnets are required per linac.

An additional possibility which has not been investigated in detail, is to mount the quadrupole magnets on micro-movers. These micro movers are comparable to those for the FFTB [50]. This way space otherwise necessary for correction coils can be saved. A cost comparison between the two possibilities is needed before a conclusion can be drawn.

Bibliography

[1] H. Matsumoto et al, *Applications of Hot Isostatic Pressing (HIP) for High Gradient Accelerator Structure*, Proc. 1991 Part. Acc. Conf. 1008-1010, San Francisco (CA), 1991. and H. Matsumoto et al, *Dark Currents*, Proc. of the 1996 Linac Conference, CERN, Geneva 1996, to be published.

[2] W. Schwarz, *Vermessungsverfahren im Maschinen– und Anlagenbau.* Vermessungswesen bei Konrad Wittwer, Band 28, Konrad Wittwer Verlag, Stuttgart 1995.

[3] W. Schwarz, *Straightness Measurements for Accelerator Structures*, In: Proceedings of International Workshop on Accelerator Alignment, Nov. 14–17, 1995 at KEK, Tsukuba, Japan.

[4] R.B.Neal, editor: *The Stanford Two-Mile Accelerator*, Stanford University, W.A. Benjamin, Inc., New York, 1968.

[5] S.Ivanov, M.Dohlus: *Investigation of Field Asymmetries in the Asymmetric Input Coupler of the e+e- Injector Linac at DESY*, Internal Report, DESY M-95-01, January 1995.

[6] H.Deruyter, H.Hoag, K.Ko, C.Ng: *Symmetrical Double Input Coupler Developement*, SLAC-PUB-5887, August 1992.

[7] V.E.Kaljuzhny, N.Sobenin, M.Dohlus, N.Holtkamp et al., *Design and Performance of a Symmetric High Power Coupler for a 6 Meter S-Band Linear Collider Accelerating Structure*, Internal Report, DESY M-94-11, Oktober 1994.

[8] V.E.Kaljuzhny, N.Sobenin, M.Dohlus, N.Holtkamp et. al: *Investigation of a Hybrid Coupler for a 6 Meter S-band Linear Collider Accelerating Structure*, Internal Report, DESY M 96-05, April 1996.

[9] M. Dohlus: *Long range Dipole Wake in a 180 Cell Traveling Wave Section*, Internal Report, to be published.

[10] Ulla v. Rienen: *Higher Order Mode Analysis of Tapered Disc-Loaded Waveguides Using the Mode Matching Technique*, Particle Accelerators, 1993, Vol 41, pp. 173-201.

[11] THE S BAND 36 CELL EXPERIMENT. B. Krietenstein et al, *The S-Band 36 Cell Experiment* DESY-M-95-08T, Jun 1995. 3pp. Presented at 16th IEEE Particle Accelerator Conference (PAC 95) and International Conference on High Energy Accelerators (IUPAP), Dallas, Texas, May 1995.

[12] K.Bane, R.Gluckstern: *The Transverse Wakefield of a Detuned X-Band Accelerator Structure*, SLAC-PUB-5783, March 1992.

[13] M.Yamamoto: *Analysis of Detuned Structure by Open Mode Expansion*, LC95, Tsukuba, Japan, March 1995.

[14] C.Adolphsen et. al.: *Measurement of Wakefield Suppression in a Detuned X-Band Accelerator Structure*, Proceedings of the 17th International Linear Accelerator Conference, Tsukuba, Japan, August 21-26, 1994.

[15] K.Thompson et. al.: *Design and Simulation of Accelerating Structures for Future Linear Colliders*, Particle Accelerators, Vol 47, pp 65-109, 1994.

[16] R. Brinkmann, M. Drevlak and R.Wanzenberg, *Improved Beam Stability with New Parameter Set for the S-Band Linear Collider*, LINAC96, Geneva, August 1996.

[17] N. Kroll (UC, San Diego), K. Thompson, K. Bane (SLAC), R. Gluckstern (Maryland U.), K. Ko, R. Miller, R. Ruth (SLAC), *Higher Order Mode Damping for a Detuned Structure*, SLAC-PUB-6624, Aug 1994. 4pp. Contributed to 17th International Linear Accelerator Conference (LINAC 94), Tsukuba, Japan, 21-26 Aug. 1994.

[18] A.Jöstingmeier, M.Dohlus, C.Rieckmann, *Application of the Generalized Scattering Matrix Method and Time Domain Computation of the Transverse Long Range Wake in Linear Accelerator Structures*, to be published.

[19] J. Haimson, *High Duty Factor Electron Linear Accelerators*, Linear Accelerators, P. Lapostolle, A. Septier, North holland Publishing Company, Amsterdam, 1970.

[20] M.Dohlus, *Higher Order Mode Damping by Artificially Increased Surface losses* , Martin Dohlus, DESY Report, to be published.

[21] M. Dohlus, H. Hartwig, N. Holtkamp (DESY), K. Jin (Hefei, NSRL), A. Jostingmeier (DESY), V. Kalyuzhny (Moscow Phys. Eng. Inst.), A. Naboka, A. Vasyuchenko (Moscow, INR), S. Yarigin (Moscow Phys. Eng. Inst.), *High Power Test of the Iris Coating in the S-Band Linear Collider*, DESY-M-96-19, Sept. 1996.

[22] M. Dohlus, M. Marx, N. Holtkamp, P. Hülsmann, W.F.O. Müller, M. Kurz, H.-W. Glock, H. Klein: *S-Band HOM-Damper Calculations and Experiments*, Particle Accelerator Conference and International Conf. on High-Energy Accelerators, Dallas (Texas), May 1995.

[23] C. Peschke, Peter Hülsmann, W.F.O. Müller, H. Klein: *Beam Position Monitoring for SBLC Using HOM-Coupler Signals*; proceedings of the 5th European Particle Accelerator Conference (EPAC 96), Sitges (Spain), 1996

[24] V. Balakin, et al., Phys. Rev. Lett. **74**(1995)2479.
G. Bowden, et al., SLAC-PUB-6132 (1995).

[25] U. Ristau, *Optimierung und Automation der Positioniereinrichtung Micromover*, Diploma Thesis, Fachhochschule Ostfriesland FHO, Emden (1996).

[26] J. Hamsom, *High duty factor electron linac*, edit. P. Lapostolle, A.Septier, *Linear Accelerators Accelerating Structures Technology* , North Holland Publishing Company, Amsterdam 1980.

[27] J.G. Noomen, N. Geuzebroek, C. Schiebaan, *A Modular Cooling System for the MEA High Duty Factor Electron Linac*, IEEE Transactions on Nuclear Science, Vol. NS-28, No. 3, June 1981.

[28] R.F. Koontz, T.G. Lee, C. Pearson, A.E. Vlieks (SLAC), *Recent Performance, Lifetime, and Failure Modes of the 5045 Klystron Population at SLAC*, SLAC-PUB-5890, Aug 1992. 3pp, Presented at LINAC 92, Ottawa, Canada, 24-28 Aug 1992.

[29] T.G. Lee, J. V. Lebacqs, G.T. Konrad, *A Fifty Megawatt Klystron for the Stanford Linear Collider*, SLAC-Pub-3214, September 1983.

[30] T.G. Lee, G.T. Konrad, Y. Okazaki, M. Watanabe, H. Yonezawa,*The Design and Performance of a 150 MW Klystron at S-Band*, SLAC-PUB-3619, April 1985.

[31] D. Sprehn, R.M. Phillips, G. Caryotakis, *Performance of a 150-MW S-Band Klystron*, AIP Conference Proceedings 337, Pulsed RF Sources for Linear Colliders, Montauk, NY 1994, p. 43.

[32] D. Sprehn, *Final Report on the Development of a 150-MW S-Band Klystron*, to be published in Proceedings of Pulsed RF Sources for Linear Colliders, Shonan Village Center, Hayama, Kamagawa, Japan, April 8 -12, 1996.

[33] G.J. Faillon, *Short Presentation on High Peak Power TH 2153 Klystrons*, to be published in Proceedings of Pulsed RF Sources for Linear Colliders, Shonan Village Center, Hayama, Kamagawa, Japan, April 8 -12, 1996.

[34] R.B. Palmer, *Linear Collider RF: Introduction and Summary*, AIP Conference Proceedings 337, Pulsed RF Sources for Linear Colliders, Montauk, NY 1994, p. 1.

[35] P.B. Wilson,*Advanced RF Power Sources for Linacs* , to be published in Proceedings of the XVIII International Linac Conference, Linac96, Geneva, Switzerland, 26 -30 August, 1996.

[36] W. Matziol, PHILIPS Semiconductors RHW, Hamburg, *Series Production of High Power Klystrons*, talk given at the 'S-Band Linear Collider Meeting', December 7th to 8th, 1995, not published.

[37] H. Thom, IPEA, Berlin, *Automatic Klystron Exchange in the Linear Collider Tunnel* , study performed in collaboration with DESY, October, 1996, to be published.

[38] A.R. Donaldson, J.C. Cron, R.R. Hanselman, *The Second Generation SLAC Modulator*, SLAC-Pub-3993, June 1986.

[39] S. Choroba, M. Bieler, J. Hameister, Y. Chi,*A 375MW Modulator for a 150MW Klystron at the S-Band Linear Collider Test Facility at DESY*, to be published in Proceedings of the XVIII International Linac Conference, Linac96, Geneva, Switzerland, 26 -30 August, 1996.

[40] A. S. Omar and K. Schünemann, *Analysis of waveguides with metal inserts,* IEEE Trans. Theory Microwave Tech., vol. MTT-37, pp. 1924–1932, 1989.

[41] P.B. Wilson, *SLED: A Method for Doubling SLAC's Energy*, Technical Note SLAC-TN-73-15, 1973.

[42] Z.D. Farkas, *Binary Peak Power Multiplier and its Application to Linear Accelerator Design*, IEEE Trans. Microwave Theory Tech. , volume MTT-34, 1986.

[43] A. Fiebig, R. Hohbach, P. Marchand and J.O. Pearce, *Design Considerations, Construction and Performance of a SLED Type Radio Frequency Pulse Compressor using very high Q Cylindrical Cavities*, CERN-PS/87-45, presented at 1987 Particle Accelerator Conf., Wash., D.C., 1987.

[44] A. Fiebig and C. Schieblich, *A Radio Frequency Pulse Compressor for Square Output Pulses*, Proc. of EPAC, Rome, 1988.

[45] T.L. Lavine, Z.D. Farkas, A. Menegat, R.H. Miller, C. Nantista, G. Spalek and P.B. Wilson, *High-Power Radio-Frequency Binary Pulse-Compression Experiment at SLAC*, Proc. of IEEE Particle Accelerator Conference, San Francisco, 1991.

[46] G. A. Loew (ed.), *International Linear Collider Technical Review Committee Report*, SLAC-R-95-471, 1995.

[47] Z.D. Farkas, *SLEDED SLAC Beam Loading Compensation.*, SLAC–AAS–Note–86, Dec 1994.

[48] Z.D. Farkas, N. Holtkamp, private communication, Jan. 1994.

[49] N. Holtkamp and A. Jöstingmeier, *Multibunch Energy Compensation in Travelling Wave Linear Accelerators*, DESY-06-043, 1996.

[50] G. Bowden et al, *Precision Magnet Movers for the Final Focus Test Beam*, Nucl. Instr. and Meth., A368:579–592, 1996.